THESIS FOR THE DEGREE OF DOCTOR OF PHILOSOPHY

Colloidal interactions obtained from total internal reflection microscopy measurements and scattering data

Moheb Nayeri

UNIVERSITY OF GOTHENBURG

Department of chemistry

2011

ISBN 978-91-628-8314-0

Printed by Chalmers Reproservice
Gothenburg, Sweden 2011

Abstract

The scattering of radiation can be used to extract information about the interactions between colloidal ($10^{-7} - 10^{-3}$ cm radius) particles suspended in liquids. As colloidal interactions incorporate entropic effects they are weak and while system specific they are governed by a number of general mechanisms. Colloidal interactions can be studied to some extent by direct measurements or more indirectly by inferring information from measurements of some property of the system.
In this thesis the principal experimental technique has been total internal reflection microscopy (TIRM), which is a very sensitive scattering technique. It allows for measurements of interaction energies between a single colloidal sphere and a flat surface in the area of 10^{-21} Joules. TIRM has been applied to show that high concentrations of non-ionic surfactant, often used at low concentrations to sterically stabilize colloidal particles, can cause particles to become physically attached by some bridging structure between the surface and particle. Another common stabilization mechanism widely used in colloidal systems is charge stabilization, whereby dissociated surface charges result in repulsion between particles and surfaces at low concentrations of electrolyte. Using TIRM a wide range of electrolytes and ionic strengths have been investigated, showing that the range of repulsion is given by the so-called Debye length for almost all situations that can be studied by TIRM. The exception is shown to be higher concentrations of 2:2 electrolytes, like $MgSO_4$ and $ZnSO_4$, in which repulsions are longer-ranged than expected.
At high electrolyte concentrations attractive van der Waals interactions become important. When the interaction involves surfaces or particles of two different materials with a solvent with properties in-between those of the two materials, it is possible that the van der Waals interaction can become repulsive. Some support for this occurring in polar solvent mixtures under special conditions has been obtained by TIRM.
Small colloidal particles can be used to induce effective interactions between larger particles and surfaces. A widely studied mechanism is depletion, which results from the imbalance in osmotic pressure when two surfaces come close enough together to exclude the small "depletant" spheres from the gap in between. TIRM was used to study the effect of concentration of charged depletant spheres and electrolyte on the depletion-like structural interactions between a large colloidal sphere and a flat surface. At high depletant concentrations an attraction is observed followed by a repulsive barrier as a function of separation distance, which is modeled using integral equation theory. Integral equation theory has also been used in modeling the interactions between oil-swollen surfactant micelles, so-called microemulsion droplets, based on non-ionic surfactant in water. Small-angle X-ray scattering data for a range of droplet concentrations were shown to be well described by a model based on an effective hard-sphere interaction, i.e. a short-ranged highly repulsive interaction, which is an example of an indirect method of obtaining information on colloidal interactions.

List of Papers

Paper I	**Surfactant effects on colloidal interactions: Concentrated micellar solutions of nonionic surfactant** M. Nayeri, R. Karlsson, J. Bergenholtz *Colloids and Surfaces A: Physicochem. Eng. Aspects* **368**, 84-90 (2010)
Paper II	**Measurements of screening length in salt solutions by total internal reflection microscopy** M. Nayeri, Z. Abbas, J. Bergenholtz *submitted to J. Phys. Chem. C*
Paper III	**Total internal reflection microscopy measurements of low-refractive index particles suspended in polar solvent mixtures** M. Nayeri, J. Bergenholtz *Manuscript*
Paper IV	**Effects of salt and particle concentration on the effective wall-sphere interaction in charged colloidal particle mixtures** M. Nayeri, J. Nordström, J. Bergenholtz *Manuscript*
Paper V	**Scattering functions of core-shell-structured hard spheres with Schulz-distributed radii** M. Nayeri, M. Zackrisson, J. Bergenholtz *J. Phys. Chem. B*, **113**, 8296-8302 (2009)

Publication not included in the thesis

Concentration- and pH-dependence of highly alkaline sodium silicate solutions, J. Nordström, E. Nilsson, P. Jarvol, M. Nayeri, A. Palmqvist, J. Bergenholtz, A. Matic, *J. Colloid Interf. Sci.*, **356**, 37-45 (2011)

Contribution report

`Paper I`
I planned and performed the majority of the experiments, analyzed the experimental results, and wrote some sections of the paper.

`Paper II`
I planned and performed all the experiments, wrote some of the programs for the data analysis, and wrote the first draft of the paper.

`Paper III`
I planned and performed all the experiments, wrote the programs for the data analysis, and wrote the first draft of the paper.

`Paper IV`
I planned and performed the majority of the experiments and wrote the first draft of the paper.

`Paper V`
I contributed to the derivation of the results for the theoretical model and implemented them in the MATLAB® environment.

CONTENTS

CHAPTER 1

INTRODUCTION

We come in contact on a daily basis with colloidal systems, from the milk we drink which is an example of an emulsion, to the ink dispersion in the ballpoint pens we use. Many industrial processes involve use of colloidal particles in one form or another. Examination of the definition of colloidal particles makes the importance of colloidal systems clear. Looking up the word colloid in Encyclopædia Britannica one finds the following description of the word colloid

> any substance consisting of particles substantially larger than atoms or ordinary molecules but too small to be visible to the unaided eye; more broadly, any substance, including thin films and fibres, having at least one dimension in this general size range, which encompasses about 10^{-7} to 10^{-3} cm.

With such a definition it becomes evident that work in colloid science treats and encompasses a wide range of areas and scientific disciplines, which the subheading of F. Evans and H. Wennerström's book *The Colloidal Domain* sums up as *where physics, chemistry, biology, and technology meet*.[1] With the increasing ability to study colloids due to technological advancement, a growing number of applications have emerged that use and manipulate the properties of colloidal particles. The importance of the ability to control and design colloidal particles emerges in current research areas such as fuel-cells,[2] lithium-ion batteries[3] and medicinal drug delivery.[4] Clear understanding of the fundamental sciences that govern colloids could be the deciding factor between success and failure of a particular application or product.

Since colloidal particles contain large quantities of molecules, often in an approximately fixed configuration, it proves convenient to subsume the molecular interactions by a colloid-colloid interaction. This interaction is in general a complicated quantity that incorporates effects like, e.g., the restructuring of nearby solvent molecules due to the presence of the colloidal particles, redistribution of ions in the solvent in response to the surface charge of the colloidal

particles, changes in entropy of the total system due to the position of the colloidal particles. These colloidal interactions are weak by our standard but acting in concert among many colloidal particles they produce systems with widely varying properties, leading to colloidal fluids, crystals, and gels.[5,6,7] In contrast to molecular interactions it is often possible to relatively easily change the colloidal interaction. A small change in the composition of the solvent or addition of a small amount of electrolyte can significantly change the nature of the colloid-colloid interaction.

Due to the size range of colloids and the fact that many important interactions in colloidal systems can be relatively weak, the structure and the interactions in colloidal systems are often studied indirectly. This is done for instance by studying the scattering profile of the colloidal system or measuring the rheological properties of the system and relating the result to what it would mean for the interactions in the system. Based on the results obtained one can then draw conclusions about the interactions that prevail in the system. In Paper V we studied small angle X-ray scattering data from microemulsion droplets made of a mixture of water, oil, and non-ionic surfactant, where we found the droplets to be well described as polydisperse spherical particles having short ranged, highly repulsive interactions.

There are also a few direct ways to measure forces or interaction potentials in colloidal systems. One of the most used methods of measuring interaction forces relevant to colloidal systems have during the last 40 years been the Surface Forces Apparatus (SFA).[8,9,10] The SFA measures the force between surfaces of two macroscopic cylinders of diameters of about 1 cm, which gives results that can be applied for interactions between colloidal particles. SFA measurements allow for studying forces for separation distances down to 0.1 nm, but can only detect rather strong surface interactions.[9,11,12,13]

Another widely used method of measuring interactions between two surfaces is using Atomic Force Microscopy (AFM) where a particulary relevant method is to modify the AFM cantilever by gluing a spherical particle with radius of several micrometers to the tip of the AFM probe and measure the force between the particle and a macroscopically flat surface is then measured.[14,15,16,17,18] AFM allows for measurements down to separation distances of around 1 nm but it has a better force resolution compared to the SFA.

In recent years several new methods, such as Total Internal Reflection Microscopy (TIRM),[19,20,21,22] Line Optical Tweezers (LOT)[23,24] as well as other similar methods,[25,26,27,28] have been developed based on the idea of creating a probability histogram over the position of one or several colloidal particles and using the Boltzmann distribution law to calculate the interaction energy. This methodology was first suggested in 1986 by Dennis Prieve and Barbara Alexander[29] and was later developed into the mentioned TIRM technique.[30,31] Because the Boltzmann distribution law expresses the availability of different positions and the energetic cost of being in that position compared to the sur-

rounding thermal energy, the resulting measured interaction energy is given in the gauge of k_BT. In most setups this provides access to weaker interaction energies compared with the SFA and the AFM but it also limits the interaction energies that these setups can measure as the particles do not sample often enough distances corresponding to high energy. However this means that these setups give the opportunity to specifically measure around the critical limit of some of the most important interactions in colloid science considering that for colloidal systems to be stable during at least a few days, repulsive barriers of around 5-10 k_BT are sufficient.

In Paper I we again studied interactions in non-ionic surfactant solutions; this time however we used an in-house built TIRM setup to determine the interaction between a spherical colloidal particle and a flat surface. During the work we discovered that both of the non-ionic surfactants that we used had traces of ionic species that significantly altered the interaction studied. Subsequently the ions were removed from the solution enabling study of the effect of high concentrations of non-ionic surfactants on the particle-wall interaction.

For Paper II we conducted a systematic study of interactions in colloidal systems for a range of electrolytes and ionic strengths, which represents the first TIRM study of the effect of multivalent electrolyte. This necessitated taking van der Waals interactions into account. The study in Paper III focused on the van der Waals interactions of low-refractive-index particles with plane surfaces in polar solvent mixtures. The purpose was to determine the effect of salt concentration and solvent refractive index on the interaction. Finally, in Paper IV, in which particles of low refractive index were also used, the effect of concentration of small spherical particles and salt on the interaction between a large sphere and a surface was studied, an interaction that usually is called depletion.

CHAPTER 2

COLLOIDAL INTERACTIONS

As mentioned in the introduction chapter, the interaction forces in a colloidal system incorporate entropic effects and are due to the total change of the Gibbs free energy G of the colloidal system with respect to a change of the position h of a colloidal particle,

$$F = -\Big(\frac{\partial G}{\partial h}\Big)_T = -\Big(\frac{\partial H}{\partial h}\Big)_T + T\Big(\frac{\partial S}{\partial h}\Big)_T. \tag{2.1}$$

For a near incompressible solvent such as for aqueous solutions at room temperature and atmospheric pressure, one could equally well replace the Gibbs free energy with the Helmholtz free energy A, as enthalpy $H = U + pV$ only differs from the internal energy U by a constant.[1] There are many types of interactions and effects that could contribute to the change of the free energy. To account for these interactions fully analytically is more or less impossible and even numerical calculations of these interactions are likely not feasible. In many cases some simplification is needed to be able to model and predict behavior in more complex systems. In this chapter a short theoretical description of the colloidal interactions that are important for this thesis are discussed.

2.1 Hard-sphere interaction

The most simple way to account for inter-colloidal excluded volume interactions is to model these as a hard-sphere interaction, whereby the particles more or less act like billiard balls that only interact with each other by elastic collisions. Mathematically, the hard-sphere potential energy $\phi(r)$ between two spherical particles can be expressed as

$$\phi(r) = \begin{cases} \infty & \text{if } r \leq a_1 + a_2 \\ 0 & \text{if } r > a_1 + a_2 \end{cases} \tag{2.2}$$

where a_1 and a_2 are the radii of the particles and r is the center-center distance between the particles. As will be seen in chapter 3.2.1 and Paper V modeling interactions in this simple way can still lead to complex expressions for many-particle systems, especially at higher concentrations, that require numerical solutions. In some cases these expressions can be solved analytically. To include more long-range interactions and still being able to keep the simple hard-sphere interaction one can in some cases also in the modeling process make a distinction between the actual particle radius and the hard-sphere interaction radius. This leads to a so-called effective hard-sphere interaction,[32] which we introduce in Paper V to capture effects of additional repulsive interactions on the scattering properties of colloidal spheres.

2.2 Electrostatic interaction

Electrostatic forces arise from the charge that colloidal particles carry. Most colloids, especially in water with its high dielectric constant, acquire a surface charge. The surface charge is formed either by dissociation of surface groups known as ionization or by adsorption of ions onto the previously uncharged surface. This surface charge will attract a higher concentration of counterions, forming two layers, one which is the Stern layer where the ions are essentially immobile and the other layer which is known as the diffuse layer. The two layers together with the surface charge form what is known as the electrical double layer (EDL) which is electrostatically neutral. A repulsive force arises between two colloidal particles with uniform surface charge of the same sign or a charged colloidal particle and a neutral colloidal particle when they come close to each other. This force is also known as the EDL force. In 1932 Debye and Hückel derived expressions for activity coefficients of ionic species in electrolyte solutions in an article where they put forward what became known as the Debye-Hückel theory of electrolyte solutions.[33] Here they identified the screening length $1/\kappa$ as given by

$$\kappa^2 = \sum_j \frac{(z_j e)^2 n_j}{\varepsilon_r \varepsilon_0 k_B T}, \tag{2.3}$$

in terms of the valence z_j and bulk concentration n_j (molecules per cubic meter) of the jth ionic component, with ε_r denoting the dielectric constant of the solvent, ε_0 is the permittivity of free space, k_B is the Boltzmann constant and T is the temperature. It can be shown that the length scale of the EDL interaction is given by this Debye screening length, $1/\kappa$.
One can arrive at the expression for the Debye screening length and put it into context when deriving the Poisson-Boltzmann (PB) equation by combining Poisson's equation

$$-\epsilon_r \epsilon_0 \nabla^2 \Psi(r) = \rho(r), \tag{2.4}$$

which gives the relation between the electrostatic potential $\Psi(r)$ and the charge density $\rho(r)$, with the Boltzmann distribution to account for the ion concentration away from a charged spherical particle of radius a.[34] Assuming that the ions do not perturb their local environment with their size and charge, the Boltzmann distribution is given by

$$\rho(r) = \sum_j z_j n_j e \exp\Big(\frac{-z_j e \Psi(r)}{k_B T}\Big). \tag{2.5}$$

Combining these two equation we arrive at the PB-equation:

$$\nabla^2 \Psi(r) = -\sum_j \frac{z_j n_j e}{\varepsilon_r \varepsilon_0} \exp(\frac{-z_j e \Psi(r)}{k_B T}). \tag{2.6}$$

Linearizing this equation gives

$$\nabla^2 \Psi(r) = \kappa^2 \Psi(r), \tag{2.7}$$

and solving it for a constant charge boundary condition leads to

$$\Psi(r) = -\frac{Q}{4\pi\varepsilon_r\varepsilon_0(1+\kappa a)} \cdot \frac{\exp(-\kappa(r-a))}{r} \quad \text{for } r \geq a, \tag{2.8}$$

where we denote the surface charge as Q. Here the Debye length $1/\kappa$ determines the extent to which the surface potential is screened.

2.2.1 Electrostatic double layer interaction between a spherical particle and a surface

Going on to describing the electrostatic interaction between a spherical colloidal particle and a flat plate, which is of most importance for this thesis, we will again see that given some approximations, the Debye screening length sets the range of the interaction potential. To solve this problem we first look at the EDL interaction between two parallel plates $\phi(h)_{p-p,\mathrm{el}}$, with the plates having surface charges of equal sign but different magnitude of surface charge.[35,1,36] The interaction force between the plates is obtained by looking at the change in the Gibbs or Helmholtz free energy as discussed for equation (2.1):

$$\frac{\phi_{p-p,\mathrm{el}}}{\text{area}} = \int_h^\infty (\Pi_{osm}(x_0) - \Pi_{osm}(\text{bulk}))dx_0 = k_B T \int_h^\infty \sum_j (n_j(x_0) - n_j)dx_0, \tag{2.9}$$

where x is the perpendicular axis to the plates and x_0 is the position where the electric field $E = d\Psi(x)/dx$ vanishes. We can solve this problem by making some assumptions and approximations.[1,37] First, a series expansion of the

solution to PB-equation for a semi-infinite plate with constant surface potential is used

$$\Psi(x) = \frac{2k_BT}{ze}\ln\Big[\frac{1+\Gamma\exp-\kappa x}{1-\Gamma\exp-\kappa x}\Big] \approx \frac{4k_BT}{ze}\Gamma\exp-\kappa x, \tag{2.10}$$

$$\Gamma = \tanh\Big(\frac{ze\Psi_0}{4k_BT}\Big), \tag{2.11}$$

where z is the valence of a z:z symmetric electrolyte solution and Ψ_0 is the constant surface potential. Assuming linear superposition between the two potentials away from each surface with weakly overlapping EDL,[38] leads to the following solution for the EDL interaction energy between two plates

$$\frac{\phi_{p-p,\mathrm{el}}}{\mathrm{area}} = 32\epsilon_r\epsilon_0\Big(\frac{k_BT}{e}\Big)^2\kappa\Gamma_1\Gamma_2\exp(-\kappa x). \tag{2.12}$$

To go from the plate-plate interaction to a spherical particle and a plate, Derjaguin's approximation can be used which gives the interaction between two spheres with radius a_1 and a_2

$$\phi_{s-s}(h) = -2\pi\frac{a_1a_2}{a_1+a_2}\int_h^\infty \phi_{p-p}(h')dh', \tag{2.13}$$

where $h = r - a_1 - a_2$. This approximation is valid when the radius of the colloidal spheres $a_1, a_2 \gg h$. Putting $a = a_1$, $a_2 = \infty$ and $h = r - a$ gives us the relation between a sphere and semi-infinite wall. Using the Derjaugin approximation on equation (2.12) gives that

$$\phi_{s-p,\mathrm{el}} = 64\pi a\epsilon_r\epsilon_0\Big(\frac{k_BT}{e}\Big)^2\Gamma_s\Gamma_p\exp(-\kappa h). \tag{2.14}$$

Once again equation (2.14) shows how the Debye screening length $1/\kappa$ sets the characteristic range of the interaction.

2.2.2 Shortcomings of the PB theory and Debye length expression

The PB theory is a continuum theory which treats ions as point charges. It neglects the fact that charges are discrete and it neglects the molecular nature of the solvent. In addition, charges near interfaces between media of different dielectric constants experience so-called image forces, which are neglected in the PB theory. Perhaps most importantly it is a mean-field theory which means that correlations between charges are absent. This is a serious flaw when charges are strongly interacting, which occurs between multivalent ions at high concentrations. For such cases, one can expect deviations in the screening length from the expression given by the DH formula.

2.3 van der Waals interaction

In 1881 Dutch scientist Johannes Diderik van der Waals suggested weak attractive interactions between molecules as a way to explain deviations between properties of real gases and ideal gases. These interactions are known now as van der Waals (vdW) interactions and are caused by dipole interactions between molecules, either through permanent or induced dipoles. Even if two molecules are nonpolar, a dipole-dipole interaction will arise between the two, due to quantum fluctuations in electron density of the molecules which will give rise to a net attractive interaction between the molecules. The orientationaly averaged vdW-interaction is always attractive between two molecules that interact in vacuum and can be divided into three contributions. These three interaction terms are dipole-dipole (Keesom interactions), dipole-induced dipole (Debye interactions) and induced dipole-induced dipole interactions (London dispersion interactions). Disregarding the finite speed of light, i.e. retardation,[39] all the three interaction terms that are part of the vdW-interaction vary as the inverse-sixth power ($-C/r^6$) of distance r when Boltzmann averaged over different rotational angles, with C being a constant accounting for the contribution from the constants of all three interactions.
In 1937 H. C. Hamaker,[40] assuming pair-wise additivity of the vdW-interactions between molecules, reached the result that for two semi-infinite plates, the $-C/r^6$ molecular interaction results in a total interaction between the plates per unit area that decays as the inverse-square power of distance,

$$\frac{\phi_{p-p,\mathrm{vdW}}}{\text{area}} = -\frac{H}{h^2}, \tag{2.15}$$

where H is the Hamaker constant and h is the distance between the semi-infinite plates. For two equally sized spherical particles Hamaker showed that at shorter distances (where the sphere radius is $R \gg h$) the interaction decays as slow as the inverse of the distance $-H/h$ while for longer distances ($R \ll h$) one gets back the $-H/h^6$ decay. The expression for the vdW-interaction between a sphere and a surface, which is of particular interest for this thesis, is either calculated by Derjaugin's approximation from equation (2.13) which gives

$$\phi_{s-p,\mathrm{vdW}}(h) = -\frac{Ha}{6h}, \tag{2.16}$$

or by an empirical adaptation of Hamaker′s linear superposition formula

$$\phi_{s-p,\mathrm{vdW}}(h) = -\frac{H}{6}\left[\frac{a}{h} + \frac{a}{h+2a} + \ln\left(\frac{h}{h+2a}\right)\right]. \tag{2.17}$$

As equations (2.15) and (2.17) show, the vdW-interactions in colloidal systems can be quite long range. It is this realization together with the expression for the EDL interaction that resulted in DLVO-theory derived during the

1940s. Neglecting other types of interactions and summing the attractive vdW-interaction and the repulsive EDL interaction, yields the DLVO-theory, the first theory that managed to successfully describe colloidal stability.
However, there are approximations in Hamaker′s derivation. The major problem comes from assuming pairwise additivity. Neglecting the finite speed of electromagnetic waves and not including screening are the other sources of error.

2.3.1 Retardation, non additivity and screening of van der Waals interaction

In the non-retarded case the vdW-interaction between two molecules decays as $-1/r^6$. In 1946 Casimir and Polder[39] showed that while this holds true at shorter distances, for distances around 10 nm and beyond, the finite speed of electromagnetic waves need to be accounted for, which results in so-called retardation. Taking into account retardation, the London dispersion part of the vdW-interaction decays more rapidly, as the inverse seventh power of distance ($-1/h^7$) for interactions over larger distances. This comes from the fact that the vdW-interaction has to do with the synchronized charge fluctuation in molecules. For shorter distances the time for a molecule to "see" changes in the charge distribution around another molecule is almost instant, while for longer distances the finite speed of light gives a lag in this correlation. This applies only for the London dispersion force as the time scale for fluctuations in electron density can compare with lag time due to the finite speed of electromagnetic waves, while dipole rotations occur on slower time scales. As the London dispersion is usually the dominant part of the whole vdW-interaction, the distance dependence of the vdW-energy between two atoms progresses as: $-1/h^6 \rightarrow -1/h^7 \rightarrow -1/h^6$. For longer distances when the London dispersion part has decayed, the whole of the vdW-interaction again begins to decay as $-1/h^6$.
The major problem with Hamaker's derivation of a Hamaker constant is that it suffers from the assumption of pair-wise additivity, which ignores the influence of neighboring atoms on the interactions that is being summed between the atom pairs.This problem was altogether circumvented by the macroscopic approach taken in Lifshitz theory[41,42] where the starting point is not the interaction between molecules, but the dielectric response function of a whole medium. The dielectric function $\epsilon(\nu)$, also known as permittivity, describes how a medium responds to an electromagnetic field, with ν being the frequency of the applied electromagnetic field. This approach is a continuum approach that does not capture interactions between particles at distances close to atomic scales, but gives rigorous results for larger length scales.
The original Lifshitz theory is based on quantum field theory and gives the vdW interaction as a function of distance between medium 1 and 3, with 2

being the intermediate medium.[41,42] For flat semi-infinite plates the Hamaker function is determined as[43]

$$\begin{aligned} H_{123}(h) &= -\frac{3}{2}k_BT\sum_{n=0}^{\infty}{}' \int_{r_n}^{\infty} x\{\ln[1-\triangle_{12}\triangle_{23}e^{-x}] + \\ &\quad \ln[1-\overline{\triangle}_{12}\overline{\triangle}_{23}e^{-x}]\}dx \end{aligned} \tag{2.18}$$

$$\begin{array}{ll} \triangle_{jk} = \frac{\epsilon_j s_k - \epsilon_k s_j}{\epsilon_j s_k + \epsilon_k s_j} & \overline{\triangle_{jk}} = \frac{s_k - s_j}{s_k + s_j} \\ s_k^2 = x^2 + \left(\frac{2\nu_n h}{c}\right)^2(\epsilon_k - \epsilon_3) & r_n = \frac{2h\nu_n\sqrt{\epsilon_3}}{c} \\ \nu_n = \frac{2\pi n k_B T}{h_p} & \epsilon_k = \epsilon_k(i\nu) \end{array}$$

where the Planck constant is denoted as h_p, while keeping h as the separations distance, $\epsilon_k(i\nu_m)$ is the dielectric response of medium k to the electric field of frequency $\nu_m = 2\pi k_B T m/h_p$, and $i = \sqrt{-1}$. The prime ($'$) on the sum denotes that the first term is to be multiplied by $(1/2 + \kappa h)\exp(-2\kappa h)$ to account for screening of the static part of the vdW interaction.
While the London dispersion part is subject to retardation, the zero frequency part of the Hamaker constant, i.e. mostly the Keesom (dipole-dipole) and Debye (dipole-induced dipole) interaction parts are subject to screening in electrolyte solutions. This comes from the fact that the angle-averaged Keesom and Debye interactions are basically electrostatic interactions and therefore subject to screening, similar to the screening discussed in section 2.2. In most systems the zero-frequency part of the vdW interaction gives a weaker contribution to the vdW interaction, and screening can thus be omitted. However in systems where the London dispersion part is less dominant or even weaker than the two other contributions, such as for interactions between polymer particles in water, screening cannot be excluded.

2.3.2 Simplifications to Lifshitz equation

To solve (2.18) one needs to know the dielectric response function for all three media over a wide frequency range, something that is not feasible for most materials. However, Parsegian and co-workers have shown that calculations with reasonable accuracy can be achieved even when the dielectric spectra are far from complete.[44,45] In many instances, it has been shown that it is a reasonable approximation to model the dielectric response function by a damped oscillator model in the form of[44,46]

$$\epsilon(i\nu_m) = 1 + \frac{B}{1+\nu_n\tau} + \sum_j \frac{C_j}{1+(\nu/\omega_j)^2 + g_j\nu/\omega_j^2}, \tag{2.19}$$

where $1/\tau$ is the microwave decay amplitude, ω_j is the oscillator frequency, g_j is the bandwidth of the relaxation and C_j is related to the oscillator decay amplitude. The first term after unity includes the contribution of permanent

dipoles, which is an important contribution for polar solvents. Bergström has summarized values for these parameters for some of the most common materials.[47]
Still, the dielectric response function of many materials is not characterized over quite enough frequency range. For some materials the following equation can suffice

$$\epsilon(i\nu) = 1 + \Big(\frac{n^2 - 1}{1 + \nu^2/\nu_e^2}\Big), \tag{2.20}$$

where n is the refractive index of the material in the visible regime and ν_e is the main electronic absorption frequency. Nevertheless to calculate the full Lifshitz equation with retardation is difficult for most material systems and impossible for some, and even more so if the interaction involves other geometries than two homogenous smooth plates. It is then easier to use a modified Hamaker approach to calculating of the vdW interaction. To include retardation in the Hamaker approach, Schenkel and Kitchener[48] derived an expression for the London dispersion interaction energy $U(h)$ between two atoms as

$$U(h) = -\frac{B}{h^6}\Big(\frac{2.45}{p} - \frac{2.17}{p^2} + \frac{0.59}{p^3}\Big), \tag{2.21}$$

where $p = 2\pi h/\lambda$, with λ being the intrinsic electronic oscillation wavelength of the atoms. Based on this expression for the London dispersion energy the vdW interaction between two semi-infinite walls, which before in the Hamaker derivation was given by equation (2.15), now becomes

$$\frac{\phi_{p-p,\mathrm{vdW}}(h)}{\text{area}} = -\frac{H}{h^3}\Big(\frac{2.45\lambda}{60\pi^2} - \frac{2.17\lambda^2}{240\pi^3 h} + \frac{0.59\lambda^3}{840\pi^4 h^2}\Big) \tag{2.22}$$

As the value of λ is largely unknown, one can use it as a fitting parameter to fit the above expression against the full Lifshitz expression for the plate-plate geometry. The same λ is then used for more complicated geometries.[49]
It should also be pointed out that expressions given in this section have been for interactions for smooth surfaces, which except for the atomically smooth mica sheets used in SFA measurements are perhaps not appropriate for other direct force measurements. Therefore results of measuring directly the vdW interaction may deviate from theory. Models have been developed to include surface roughness which ultimately gives another fitting parameter for the experimental results.[50,49,51] In Paper II we chose to treat the vdW interaction in accordance with a surface roughness model proposed by Walz et al.[52,53,49]
A simplification which can be made in order to get an overview of vdW interaction between three media is to use the result of equation (2.20), together with the assumption that the electronic absorption frequency ν_e is the same for all three media and put into a simplified version of equation (2.18), which results

in the following expression[54]

$$H_{123} = \frac{3}{4}k_BT\Big(\frac{\epsilon_1-\epsilon_2}{\epsilon_1+\epsilon_2}\Big)\Big(\frac{\epsilon_3-\epsilon_2}{\epsilon_3+\epsilon_2}\Big) + \frac{3h\nu_e}{8\sqrt{8}}\frac{(n_1^2-n_2^2)(n_3^2-n_2^2)}{\sqrt{(n_1^2+n_2^2)(n_3^2+n_2^2)}\{(n_1^2+n_2^2)^{1/2}+(n_3^2+n_2^2)^{1/2}\}} \quad (2.23)$$

As seen, the Hamaker constant is divided into two parts. The first is a zero-frequency term and the second is a high frequency term. It can be seen from equation (2.23) that with $\epsilon_1 > \epsilon_2 > \epsilon_3$ and $n_1 > n_2 > n_3$ the total Hamaker constat would be repulsive. The thought of a repulsive vdW interaction between two particles in a solution may seem perplexing but can most easily be viewed as an electromagnetic equivalent of Archimedean buoyancy.[55] In polar solvents with high dielectric constants the first term can seldom become repulsive. However with a repulsive high-frequency term and with the screening only effecting the zero-frequency term, the net vdW interaction can be made repulsive or to go from attractive to repulsive by increasing the ionic strength. Even though the phenomenon of repulsive vdW interaction has been known since the formulation of Lifshitz theory, direct measurements of it have been rare.[56,57,58,59,60] Few measurements of repulsive vdW interactions have been reported where the intermediate medium is polar liquid. We have in Paper III investigated vdW interaction in systems with polar solvents where equation (2.23), with a screened zero-frequency term, would suggest a repulsive vdW interaction.

2.4 Depletion interaction

Depletion interactions were first described in 1925[61] as it was observed that adding soluble polymers to a colloidal mixture led to aggregation of the colloids. A theoretical description for this phenomena was given first in 1954 by Asakura and Oosawa[62] and independently in 1976 by Vrij.[63] The mechanism behind depletion can be understood by considering figure 2.1, where the osmotic pressure outside the gap between the larger particles is larger thus resulting in an attractive interaction between the particles.
At the same time this interaction can be repulsive for longer ranges if a few of the smaller surrounding particles, referred to as depletants, come into the gap, hindering the larger particles from coming closer to each other.
The first theoretical treatment of depletion interactions considered depletion with non-adsorbing polymers as the depletants. Vrij modeled these polymers as an ideal gas but with a hard sphere interaction with the surfaces. Even though the expressions he derived are successful in many cases, they neglect depletant interactions and a more sophisticated theory is needed for more complex systems.[64,65] In our work we have measured depletion interactions induced by the depletants that are spherical particles with a surface charge. We have

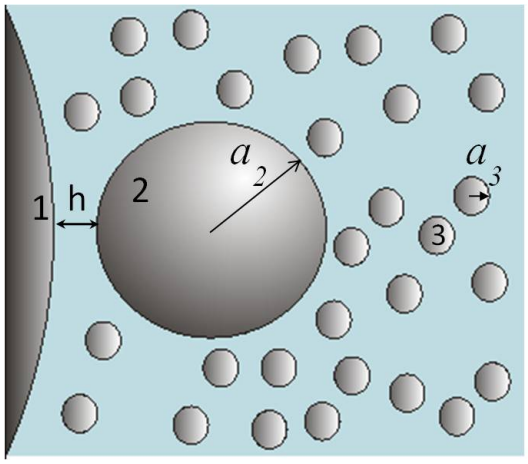

Figure 2.1: Schematic over depletion interaction between two larger spherical particles surrounded by spherical depletants.

adopted the method of Méndez-Alcaraz and Klein[66] and use integral equation theory[67] to obtain the effective interaction between a single particle and a wall in a mixture of charged monodisperse depletant particles.

2.4.1 Depletion-like interaction calculated by integral equations

The Ornstein-Zernike (OZ) equation is a statistical mechanical approach that uses integral equation theory in accounting for the inter-particle correlations.[67] The OZ equation for a discrete mixture is given as

$$h_{ij}(r) = c_{ij}(r) + \sum_{k=1}^{m} n_k \int d\mathbf{r}' h_{ik}(|\mathbf{r} - \mathbf{r}'|) c_{kj}(\mathbf{r}'), \tag{2.24}$$

where $h_{ij}(r)$ is the total correlation function of a particle of type i interacting with a particle of type j distance r away. This is done in OZ equation by dividing $h_{ij}(r)$, in two parts, one part expressing the direct correlation between particles of type i and j distance r apart, and the other part expresses the influence of the correlation of the other particles on particles i and j . In our case we have limited the mixture to three components, with component 1 being the wall, component 2 the large spherical colloid, and component 3 being the depletant particles. This treatment disregards polydispersity of the depletant particles. Furthermore to be able to keep the problem in spherical coordinates the wall itself is modeled also as a spherical particle, but with a much larger diameter than for component 2 and 3, making its curvature almost flat in comparison. Equation (2.24) can be Fourier transformed by multiplying

it with $e^{-i\mathbf{q}\cdot\mathbf{r}}$ and integrating in following way

$$\begin{aligned}\int d\mathbf{r}e^{-i\mathbf{q}\cdot\mathbf{r}}h_{ij}(r) &= \int d\mathbf{r}e^{-i\mathbf{q}\cdot\mathbf{r}}c_{ij}(r) \\ &\quad + \sum_{k=1}^{3} n_k \int d\mathbf{r} \int d\mathbf{r}' e^{-i\mathbf{q}\cdot(\mathbf{r}-\mathbf{r}')}h_{ik}(|\mathbf{r}-\mathbf{r}'|)e^{-i\mathbf{q}\cdot\mathbf{r}'}c_{kj}(\mathbf{r}') \\ \tilde{h}_{ij}(q) &= \tilde{c}_{ij}(q) + \sum_{k=1}^{3} n_k \tilde{h}_{ik}(q)\tilde{c}_{kj}(q). \end{aligned} \tag{2.25}$$

Here $\mathbf{q}$ is the wave vector which is given in the reciprocal space. As n_k expresses the number density of each component and $n_1, n_2 \to 0$, each total correlation function given in equation (2.25) is reduced to a sum of two parts. We write down the total correlation function between the wall and the large colloidal particle which is of most interest for us. With

$$\tilde{h}_{13}(q) = \frac{\tilde{c}_{13}(q)}{1 - n_3\tilde{c}_{33}(q)},$$

we get

$$\begin{aligned}\tilde{h}_{12}(q) &= \tilde{c}_{12}(q) + \frac{n_3\tilde{c}_{13}(q)\tilde{c}_{32}(q)}{1 - n_3\tilde{c}_{33}(q)} \\ &= \tilde{c}_{12}^{\text{eff}}(q) \end{aligned} \tag{2.26}$$

To solve the OZ equations we have to relate $h_{ij}(r)$ and $c_{ij}(r)$ to each other through additional, invariably approximate equations, known as closures. Different closures are suitable for different systems. We used a hybrid closure relation consisting of the hypernetted chain (HNC) closure, and the mean spherical approximation (MSA). The HNC closure is usually well suited for long-range potentials, and in particular electrostatic interactions[67] and is given by:

$$c_{ij}(r) = -\frac{\phi_{ij}(r)}{k_B T} + h_{ij}(r) + \ln(1 + h_{ij}(r)). \tag{2.27}$$

where $\phi_{ij}(r)$ is the pair potential. We modeled this interaction as a combination of the hard-sphere interaction given in equation (2.2) and the EDL interaction

$$\phi_{ij}(r) = \begin{cases} \infty & \text{if } r \le a_i + a_j \\ \frac{e^2 Q_i Q_j}{4\pi\varepsilon_0\varepsilon_r(1+\kappa a_i)(1+\kappa a_i)r} e^{-\kappa(r-a_i-a_j)} & \text{if } r > a_i + a_j \end{cases} \tag{2.28}$$

We used the HNC closure for all components except for the correlation between component 1 and 2, where the MSA closure was used. The MSA is given by

$$\begin{aligned} c_{12}(r) &= -\frac{\phi_{ij}(r)}{k_B T} \\ c_{12}^{\text{eff}}(r) &= -\frac{\phi_{12}^{\text{eff}}(r)}{k_B T}. \end{aligned} \tag{2.29}$$

Solving the OZ equation (2.24) for our 3-component system and obtaining results for $c_{12}^{\text{eff}}(r)$ gives us the sought after interaction between the wall and the larger colloidal sphere as $\phi_{12}^{\text{eff}}(r)$.

CHAPTER 3

SCATTERING

Different scattering techniques are essential when probing the structure and interactions in colloidal systems. The scattering here refers to the elastic or quasi-elastic scattering of light or neutrons. There are many different types of setups and techniques using scattering even when limiting the discussion to elastic or quasi-elastic scattering, but the focus in this chapter will be the two scattering techniques that have been used in this thesis, i.e. evanescent scattering in the TIRM technique and small-angle X-ray and neutron scattering.

3.1 Evanescent scattering

Scattering from an evanescent electromagnetic field is a central part in the main instrument used in this thesis, namely Total Internal Reflection Microscopy (TIRM). In TIRM laser light is totally reflected at an interface between two different media, with the first medium having a higher refractive index than the latter. In TIRM, medium 1 is usually a glass prism that is optically coupled to a glass cell, which contains the solution that serves as medium 2 and as said $n_1 > n_2$, as shown schematically in figure 3.1. Even if the name total internal reflection suggests that all light will be reflected at the interface, an electromagnetic field will still penetrate into medium 2. Mathematically this is due to boundary conditions at the interface and a more physically oriented explanation of this phenomena is that the electromagnetic field cannot be discontinuous at the boundaries. The created electromagnetic field, called the evanescent wave, differs from the incident and reflected waves in that it propagates parallel to the interface while the amplitude decays exponentially with the distance measured normal to the interface. The evanescent wave will not transfer energy into the second medium unless it interacts with a third medium. In the TIRM case this medium is a spherical colloidal particle, as seen in figure 3.1.

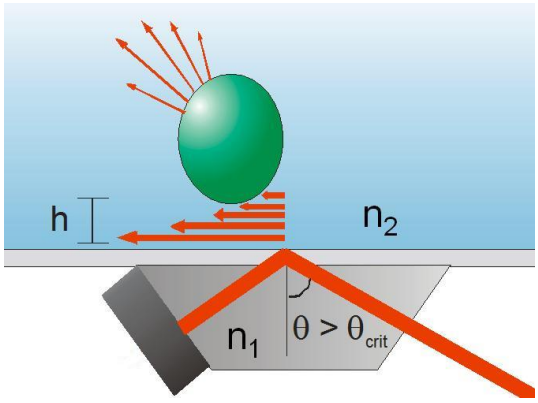

Figure 3.1: Schematic picture of the mechanism behind creating an evanescent wave at a glass-solvent interface. When the laser light is reflected at the glass-solvent boundary at an angle greater than the critical angle θ_{crit}, an evanescent wave is created in the solution. A particle that has a refractive index different from the surrounding solvent will scatter the evanescent light. In our TIRM setup an absorbing dark glass plate is placed at the end of the dovetail prism to absorb the reflected laser.

The electromagnetic field that penetrates into medium 2 will decay exponentially away from the interface. Prieve and Walz[68] building on work done by Chew et al.[69] used ray-optics to show that the intensity of the scattered evanescent wave by a colloidal sphere in the range of 3 to 30 μm also decays exponentially with distance h, i.e.

$$I = I_0 \exp(-\zeta h), \tag{3.1}$$

where ζ^{-1} is the decay length/penetration depth of the evanescent wave and I_0 is the scattered intensity at contact. Knowing the incident angle of the light source, θ_1, the decay parameter is given by

$$\zeta = \frac{4\pi}{\lambda}\sqrt{(n_1 \sin\theta_1)^2 - n_2^2}, \tag{3.2}$$

where λ is the vacuum wavelength of the light source. In addition, they demonstrated this elegantly by attaching a particle to an index-matched coating of different thicknesses. However, recent work from Helden et al.[70,71,72] suggests that this holds for p-polarized light with $\zeta^{-1} < 200$ nm, but could otherwise be false due to scattered light from the particle being back reflected at the interface. This changes the scattering profile that the light detector in the TIRM setup picks up in the forward direction.

3.2 Introduction to small-angle scattering

Just as TIRM is a scattering technique that provides information on colloidal interactions, so do other, more conventional scattering techniques, but in a far less direct way. While direct imaging of colloidal dispersions with particles in the lower end of the colloidal scale ($\approx$ 1 nm - 1 μm) is usually invasive or not available, different conventional scattering techniques provide useful physical averages for the whole system. Figure 3.2 shows the basic setup for a typical

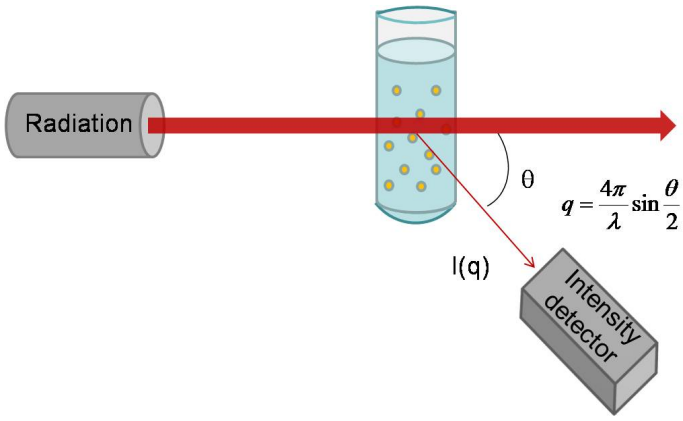

Figure 3.2: Typical setup for a scattering experiment.

static scattering experiment. A well collimated radiation source, either light, X-rays or neutrons, is made incident on a sample and the angle dependence of the average scattered intensity is determined. The angular dependence of the intensity $I(q)$ is usually expressed in terms of the scattering vector $\mathbf{q}$, which is defined as

$$\mathbf{q} \equiv \mathbf{k}_i - \mathbf{k}_s$$
$$q \equiv |\mathbf{q}| = \frac{4\pi}{\lambda} \sin\frac{\theta}{2}, \tag{3.3}$$

where $\mathbf{k}_s$ and $\mathbf{k}_i$ are the propagation vectors of the scattered and incident radiation, θ is the scattering angle, and λ is the wavelength of the radiation in the sample. We have done work in Paper V on modeling $I(q)$ based on some assumptions regarding the interaction of the colloidal particles in the studied solution as well as their shape, the results of which are most usable in small-angle scattering (SAS) experiments.

3.2.1 Small-angle scattering theory

To model scattering data quantitatively one has to describe the probability to observe scattered radiation at a given solid angle. Even though X-rays and neutrons would seem quite different as radiation sources and the treatment of the physics of how they scatter is different, their differences will not enter

besides the value and meaning of this probability. It is worth noting that for X-rays and neutrons a general valid approximation is that scattering from one source at a point $\mathbf{r}$ does not depend on scattering from other scatterers. This allows for the local scattered amplitudes,

$$F(q) = \int_V d\mathbf{r}(\varrho(\mathbf{r}) - \varrho_{solv}) \exp(-i\mathbf{q}\cdot\mathbf{r}), \tag{3.4}$$

of local scatterers to simply be added to each other, with $\mathbf{q}$ as defined in equation (3.3), $\varrho(\mathbf{r})$ is the local density of scatterers and ϱ_{solv} accounts for the background scattering of the solvent.[73] The statistical average of the scattered intensity per unit volume V is then expressed as

$$\begin{aligned} I(q) &= \left\langle \frac{F(q)\cdot F(q)^*}{V} \right\rangle \\ &= \left\langle \frac{1}{V}\int_V\int_V d\mathbf{r}d\mathbf{r}'(\varrho(\mathbf{r}) - \varrho_{solv})(\varrho(\mathbf{r}') - \varrho_{solv})e^{-i\mathbf{q}\cdot(\mathbf{r}\text{-}\mathbf{r}')} \right\rangle. \end{aligned} \tag{3.5}$$

If we take the case of scattering from N identical particles that scatter independently and introduce vectors $\mathbf{r}_i$ and $\mathbf{r}_j$ that point to the centers of particles i and j, and make the following variable change, $\mathbf{r} = \mathbf{r}_i + \mathbf{u}$ and $\mathbf{r}' = \mathbf{r}_j + \mathbf{v}$, we get that equation (3.5) becomes[74]

$$\begin{aligned} I(q) = \frac{N}{V}\Big\langle \Big\{ \int\int_{V_{part}} d\mathbf{u}d\mathbf{v}(\varrho(\mathbf{u}) - \varrho_{solv})(\varrho(\mathbf{v}) - \varrho_{solv}) \exp[-i\mathbf{q}\cdot(\mathbf{u}-\mathbf{v})] \Big\} \\ \Big\{ \frac{1}{N}\sum_{i=1}^{N}\sum_{j=i}^{N} \exp[-i\mathbf{q}\cdot(\mathbf{r}_i - \mathbf{r}_j)] \Big\} \Big\rangle, \end{aligned} \tag{3.6}$$

where V_{part} is the volume of one of the particles. Equation (3.6) is often written in the compact form

$$I(q) = nP(q)S(q), \tag{3.7}$$

where $n = N/V$ is the number density of the particles in the system, $P(q)$ is known as the form factor of the system, and $S(q)$ is the structure factor. The form factor $P(q)$ contains information about the particles shape and composition and is given by the integral part of equation (3.6) which is equivalent to $P(q) = F(q)\cdot F^*(q)$. The second term in equation (3.6) is the structure factor $S(q)$, which accounts for the inter-particle correlation in the system and gives therefore the "structure" in terms of the spatial distribution of particles in the system. The structure factor can be written as[67,75]

$$S(q) = 1 + n\int d\mathbf{r}_{12}(g(r_{12}) - 1)\exp(-i\mathbf{q}\cdot\mathbf{r}_{12}), \tag{3.8}$$

where $g(r_{12})$ is called the normalized pair distribution function which describes the probability of finding two particles at $\mathbf{r}_1$ and $\mathbf{r}_2$, in respect of the position of the other particles. The normalized pair distribution function is connected to the total correlation function given in section 2.4.1 simply as $h(r) = g(r) - 1$.

That means that the integral in (3.8) in fact gives the Fourier transform $\tilde{h}(q)$ of the total correlation function, so that

$$S(q) = 1 + n\tilde{h}(q). \tag{3.9}$$

To obtain results for $S(q)$ for a given interaction potential, again the OZ equation given in (2.24) must be solved. Wertheim[76] and Thiele[77] solved the OZ equation analytically for a monodisperse system of hard spheres, using the Percus-Yevick closure[67]

$$c(r) = \Big(1 - \exp\Big[\frac{\phi(r)}{k_B T}\Big]\Big) g(r). \tag{3.10}$$

For the hard-sphere interaction, equation (3.10) simply becomes $c(r) = 0$ for $r > 2a$.

Mixtures of particles

Systems of synthetic colloids are invariably polydisperse to some degree, at least in terms of size. This is a complicating factor that needs to be accounted for in interpreting the results from static scattering. Equation (2.24) is here in similar fashion to equation (2.25) Fourier transformed, but this time we multiply both sides of equation (2.24) with $\sqrt{n_i n_j}$ as well. After some mathematical manipulation the Fourier transformation of (2.24) can be presented as a matrix equation involving $m \times m$ matrices,

$$\begin{aligned} \tilde{H}(q) &= \tilde{C}(q) + \tilde{C}(q) \cdot \tilde{H}(q), \\ \tilde{H}(q) &= \tilde{C}(q) \cdot [E - \tilde{C}(q)]^{-1}, \end{aligned} \tag{3.11}$$

where E is the unity matrix and we have defined the matrix elements as

$$\begin{aligned} \tilde{H}_{ij}(q) &= \sqrt{n_i n_j}\tilde{h}_{ij}(r), \\ \tilde{C}_{ij}(q) &= \sqrt{n_i n_j}\tilde{c}_{ij}(r). \end{aligned}$$

Analytical solutions for $c_{ij}(r)$ and $\tilde{C}_{ij}(q)$ for hard-sphere mixtures using the Percus-Yevick closure were first derived by Lebowitz.[78] Later Baxter[79] obtained the same result but through another formalism. With this result in hand, Blum and Stell[80,81] and Vrij[82] independently obtained the matrix inversion in equation 3.11, yielding analytical expressions for $\tilde{H}_{ij}(q)$.
The scattering intensity given in equation (3.7) for a discrete mixture is then given by

$$I(q) = \sum_{i,j=1}^{m} (n_i n_j)^{1/2} F_i(q) F_j^*(q) S_{ij}(q), \tag{3.12}$$

where, analogous to equation (3.9), $S_{ij} = \delta_{ij} + \tilde{H}_{ij}(q)$, where δ_{ij} is the Kronecker delta. It follows that the intensity can be expressed as

$$I(q) = n \sum_{i=1}^{m} x_i F_i(q)^2 + n \sum_{i,j=1}^{m} (x_i x_j)^{1/2} F_i(q) F_j^*(q) \tilde{H}_{ij}(q), \tag{3.13}$$

where $x_i = n_i/n$ is the mole fraction of species i. Another way, which is not always possible in practice, is to use a continuous distribution. For a continuous distribution of particle radii the sums in (3.13) become integrals,

$$\begin{aligned} I(q) &= n \int_0^\infty da_i f(a_i) F_i^2(q) + n \int_0^\infty \int_0^\infty da_i da_j f(a_i) f(a_j) F_i(q) F_j(q) \tilde{H}_{ij}(q) \\ &= I_1(q) + I_2(q), \end{aligned} \tag{3.14}$$

where $f(a)$ is the distribution function governing the particle radii.

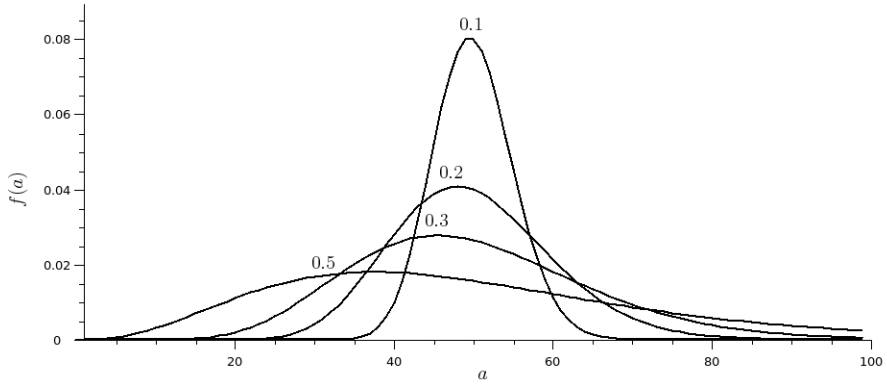

Figure 3.3: Schulz distribution, also known as Γ distribution, given by equation (3.15), where $< a >= 50$ and $s = [0.1, 0.2, 0.3, 0.5]$. Many polydisperse particle distributions in colloidal systems can be modeled quite well by the Schulz distribution.[83]

Griffith et al.[84] derived an analytical expression for the intensity in equation (3.14) for homogeneous polydisperse hard spheres when the radius distribution is given by the continuous Schulz (Γ) distribution, which is illustrated in figure 3.3. The Schulz distribution $f(a)$ of particle radii a is given by

$$f(a) = \frac{a^{c-1} \exp(-a/b)}{b^c \Gamma(c)}, \tag{3.15}$$

where $\Gamma(c)$ is the gamma function, c is related to the width of the distribution, with $c = 1/s^2$, where s is the normalized standard deviation and $b = \langle a \rangle / c$.
In our work we have obtained analytical solutions for the scattering intensity of

polydisperse core-shell and multilayered hard spheres using the Percus-Yevick closure. As a further extension of what has been done before, we have modeled the net interaction of the particles with an effective hard-sphere interaction, keeping the polydispersity governed by a Schulz distribution. This is a generalization of the results obtained by Griffith et al.[84] for homogenous polydisperse hard-sphere particles.

CHAPTER 4

TOTAL INTERNAL REFLECTION MICROSCOPY

4.1 Introduction to TIRM

The basic principle behind TIRM was suggested by Prieve and Alexander in 1986.[29] Their idea was essentially to measure repeatedly a colloid's distance from a flat wall and in this way approximate a probability function, $p(h)$, of the distance h between the colloid and the surface. Knowing the probability function one can use the Boltzmann distribution

$$p(h) = A \exp\left(\frac{-\phi(h)}{k_B T}\right), \tag{4.1}$$

to calculate the interaction energy $\phi(h)$ between the colloid and the flat surface, where A is a normalization constant, k_B is the Boltzmann constant and T is the temperature.
The way Prieve and Alexander[29,85] measured the distance was to measure the speed with which the spherical colloid is carried by a shear flow along the wall and use that to calculate the separation distance. Quite soon thereafter, in 1987, a different way of measuring this distance was suggested by Prieve et al.[30] Their new setup was in general what a TIRM instrument still is today, where properties of evanescent waves as discussed in section 3.1 is used to measure the distance between the surface and the colloidal particle. The normalization constant A can be eliminated from (4.1) by subtracting a reference interaction energy $\phi(h_m)$ from the expression which will give

$$\frac{\phi(h) - \phi(h_m)}{k_B T} = \ln \frac{p(h_m)}{p(h)}. \tag{4.2}$$

The reference h_m is usually chosen to be the height distance where the potential curve $\phi(h)$ has its minimum. Provided we have measured long enough to have good statistics, the possibility of finding the colloid at a certain height is directly

proportional to the number of observations of the colloid at that height, that is $p(h) \propto n(h)$. To go from number of observation at certain intensity to number of observation at certain distance we have following derivation:

$$\begin{aligned} n(I)dI &= n(h)dh, \\ n(h) &= -\zeta n(I)I(h), \end{aligned} \tag{4.3}$$

where equation (3.1) was used for the relation between distance and intensity. Inserting the result of equation (4.3) in equation (4.2), we get

$$\frac{\phi(h) - \phi(h_m)}{k_B T} = \ln \frac{n(I_m)I_m}{n(I)I}, \tag{4.4}$$

where $I_m = I(h_m)$. This is the central equation in the analysis of data from TIRM measurements.

4.2 The in-house-built TIRM setup

Since the TIRM instrument is built in-house, a more thorough account of the experimental setup and the procedure for the TIRM measurements will follow in this section. Figure 4.1 shows the in-house-built TIRM. Figure 4.2

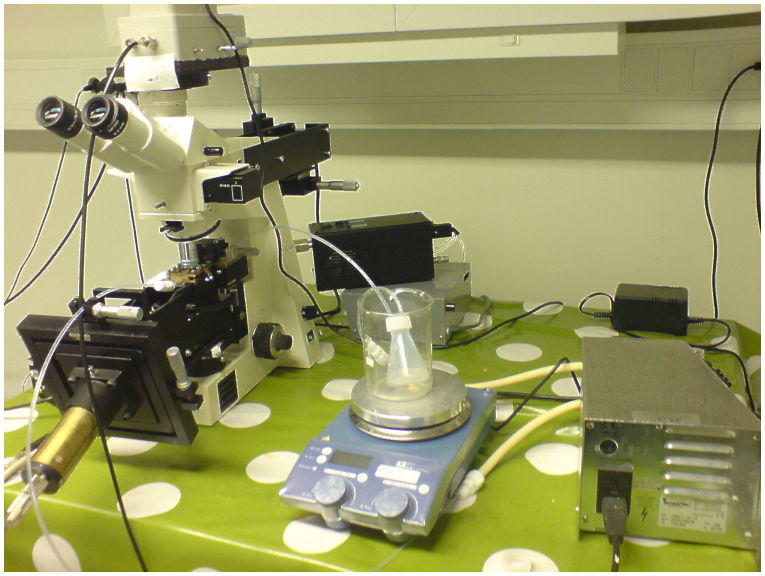

Figure 4.1: Picture of the in-house-built TIRM instrument.

shows a schematic of the setup of the TIRM equipment. We have used a Zeiss Axiolab-A microscope with a Zeiss Epiplan 50 x magnification objective as our microscope system. For creating the evanescent field, a laser diode LGTC658-50-EPS (Laser Technologies), with a wavelength of $\lambda = 658$ nm and a power

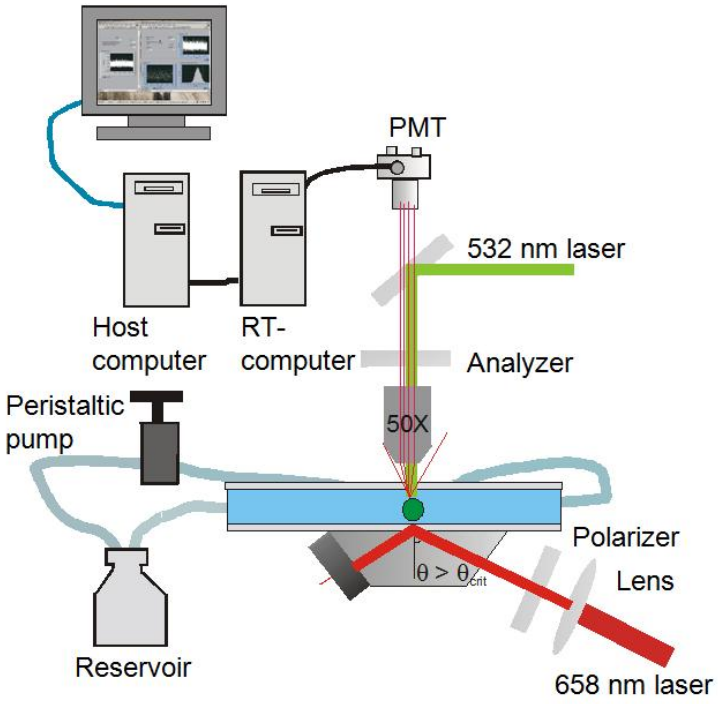

Figure 4.2: Schematic of the TIRM setup used for the work in this thesis.

of $\sim$ 33 mW is used. BK-7 dovetail prisms with angles of 72 and 75 degree (UQG Optics, refractive index of 1.515) are optically coupled to the soda lime microscope slide (refractive index of 1.513) at the bottom of the measuring cell using a immersion oil (refractive index $n = 1.518$, Zeiss). Following Bevan and Prieve,[86] the laser beam is made incident on the dovetail prism at a normal angle which assures that it will be incident on the glass-solvent interface at the angles of the dovetail prism with an estimate error of ± 0.45 degree. This is made possible by having the laser diode mounted on an arm with adjustable inclination, about 25 cm from the measuring cell. Using equation (3.2) we get decay lengths of $\zeta^{-1} = 94.3 \pm 1.5$ nm and $\zeta^{-1} = 85.6 \pm 1$nm for the 72 and 75 degree prism when the solution in the cell has a refractive index of 1.3296. The beam that is reflected at the interface strikes the other side of the dovetail prism where a neutral density absorbing filter is optically coupled to the prism, absorbing most of the beam and minimizing back reflection.
The TIRM flow cell sandwiches together two glass slides which are held approximately 4 mm apart by a rectangular rubber frame, which has two 2 mm entry and exit holes for the purpose of solvent exchange. We use a peristaltic pump (Ismatec VC-360) to connect a solution reservoir to the flow cell via teflon tubes.
As shown in figure 4.2, following procedures of other groups,[87,88] a green laser of wavelength 532 nm (Laserglow Inc.) is used to generate a two-dimensional optical trap that can hold the diffusing colloidal particle in the horizontal plane.

The green laser has variable output power, in the range of 0-150 mW, controlled by an electrical potential between 0-5 V applied over the potentiometer. Further details on how the trap works is given in section 4.2.1.
The red laser is P-polarized by a polarizer (Thorlabs). This is in accordance with work by Helden et al.[71] that shows that the intensity of the S-polarized light is more sensitive to back scattering. Reflection of the back scattered light adds to the signal and changes the exponentially decaying intensity function given in equation (3.1). As the colloidal particles studied are spherical and optically isotropic, the light scattered by the them should remain P-polarized and hence an analyzer is used to filter out any small portion of light that may have changed polarization.
We also used a bi-concave lens with a focal length of 125 mm to focus our red laser.[51,88] This leads to a focused red laser beam which increases the scattered signal form the particle and decreases the contribution of noise due to scattering from other sources than the particle. The drawback is that the intensity registered by the detector is more sensitive to lateral particle displacements.

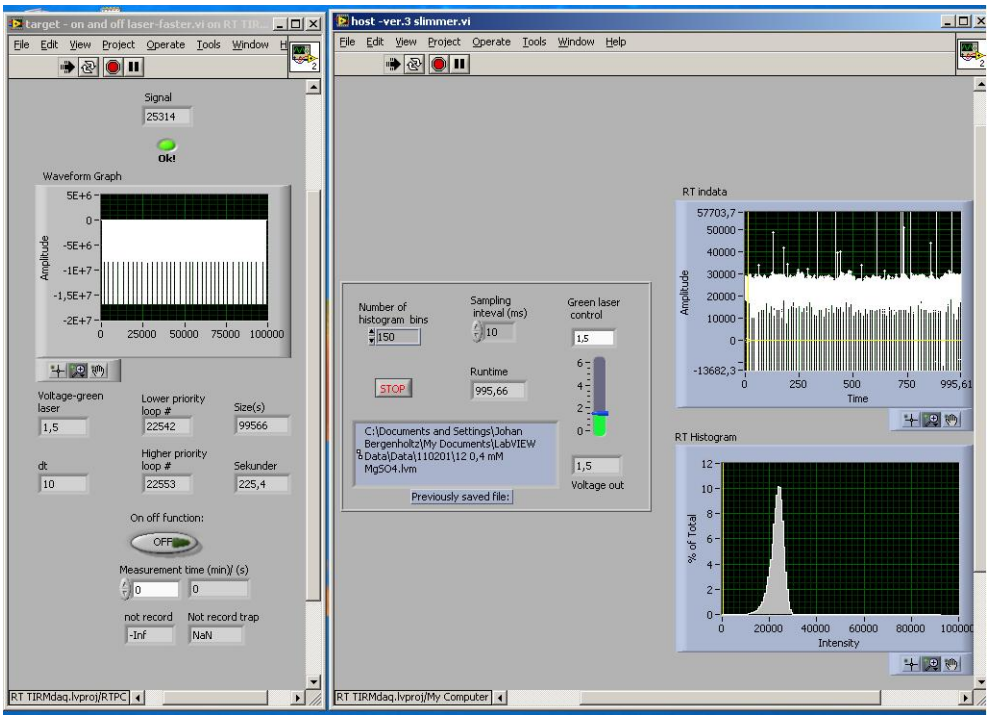

Figure 4.3: Front panel of the LabVIEW-programs used in the RT-computer (target) as well as the host computer used for recording the data.

The scattered signal is focused onto a photomultiplier tube (PMT) (Photon Technology International model PTI 810), with digital read-out, as used and recommended by Prieve and Bevan.[51] The PMT is connected through a BNC-2110 to a PCI-6024E data acquisition card (National Instruments). The card is placed in a PCI-slot of a PC, referred to as the RT(real time)-computer. The

purpose of the RT-computer is to regularly at specific time intervals, usually 10 ms, read and record the signal from the PMT. The front panel of the two programs used for this purpose can be seen in figure 4.3. Once the measurement is stopped the recorded data is sent to another PC, referred to as the host-computer, to be saved and post analyzed in programs created in the LabVIEW programming language, see section 4.3.

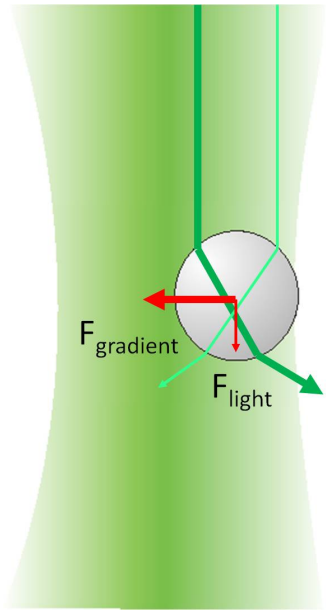

Figure 4.4: Overview figure of the mechanism behind how an optical trap works.

4.2.1 Optical trap

The optical trap serves two purposes in the TIRM setup. First it assures that the particle will remain over the same portion of the flat surface and therefore scatters evanescent light with the same zero-distance intensity, which is particulary important as the incident laser is rather strongly focused. The second purpose of the trap is to enable solvent exchange by pumping in new solvent in the cell while keeping the same particle for the next measurement. Ashkin[89] demonstrated trapping of micrometer-size colloids with dual focused lasers in 1970 and later in 1986 single-beam traps were reported.[90] The first description of using an optical trap in a TIRM setup was by Brown et al. in 1989[31] and later by Walz and Prieve in 1992.[91]
An overview of how the optical trap works on a spherical colloidal particle is given in figure 4.4. The momentum change of the photons as they are refracted at the particle-solvent interface, according to Snell's law, $n_c \sin\theta_c = n_s \sin\theta_s$, gives rise to a momentum change on the particle to conserve the total momentum. Using a laser beam with a Gaussian profile, i.e. a TEM_{00} profile, and with

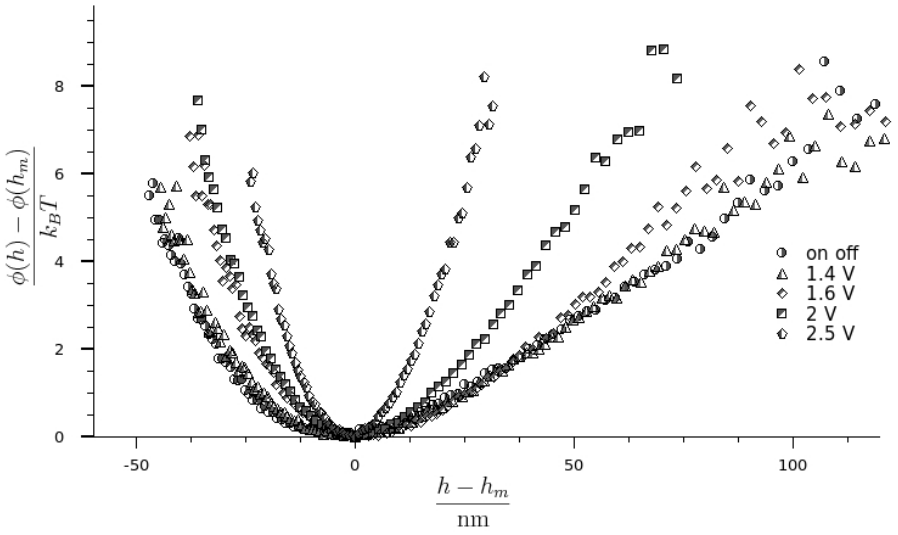

Figure 4.5: Measurements with different strength of the optical trap. The higher the applied voltage the higher the green laser power, which leads to a higher downward force. This can be seen in the curves as an increase of the positive slope. The on-off curve is a function in our TIRM setup where the trap is active in short intervals, during which no data are recorded. The measurement was done on a polystyrene particle with a diameter of approximately 10 μm in a 0.2 mM NaCl solution.

a not too strongly focused waist, the average momentum change will result in a downward force and a force toward the center of the beam profile. Even though one can simply regard the downward force as part of the gravitational force and thus subtract it from the obtained force profile, during our measurements we have tried to keep the downward force as small as possible while still having a functional horizontal trap. This is achieved in our setup simply by the long distance objective that we use in our microscope, as the green laser that acts as the optical trap comes through the objective as shown in the schematic in figure 4.2. Figure 4.5 shows how the particle becomes increasingly trapped as the power of the optical trap is increased. As seen, potentials of ≈ 1.4 V do not perturb the interaction potential, in which case the measurement lines up with the measurement done in the "on-off" mode. In the "on-off" mode, usually during intervals of 6 seconds, the trap is first on during 1 or 2 seconds to center the particle and then off to allow measurement a half second later after the trap goes off. The laser and the measurement is all controlled by programs created in LabVIEW. During the measurements usually a potential higher than 1.45 V is not used, while during exchange of the solvent a higher power for the laser is used to keep the particle in place.

Figure 4.6: Icon of some of the programs written in LabVIEW for post treatment and analysis of the gathered data during the TIRM measurement.

4.3 TIRM data analysis

In accordance with equation (4.4) the data recorded in an experiment is converted from a probability function $p(I)$ to an interaction energy $\phi(h) - \phi(h_m)$ in a LabVIEW-written program. To achieve good statistics the measurements must be done during long enough time, such that an intensity histogram is a good approximation for $p(I)$. In the TIRM technique we usually measure the intensity of the scattered light during small time intervals of about 5 to 10 ms for a total duration of about 10 minutes or more. This results in roughly 60000 measurement points or more, with which one should be able to construct an accurate histogram approximating the probability density of the scattered intensities from the colloidal particle, especially around h_m, the distance from the surface with the lowest interaction energy. However, while the statistics are quite good at distances which the particle samples frequently, the statistics are poorer for less frequently sampled distances, such that the shape of the potential curve is less trustworthy at its end points. A probability function can then be constructed as a histogram with user-specified bin number, with the default bin number being 150. The number of bins used has a small effect on the calculated $n(I_m)I_m$ which will shift the place of h_m somewhat. To obtain a better representation of the data area of interest, data points in the outer limits are usually excluded.
Figure 4.6) shows icons of some of these programs written in LabVIEW for post treatment of the gathered data and figure 4.7 shows the program interface that is used in converting the raw data to an interaction potential using equation (4.4). Preliminary data fitting and treatment of the data can also be done in the LabVIEW-written programs but for more accurate curve fitting, non-linear least squares fits to appropriate equations are done by mean square fitting the data in mainly MATLAB-written programs but also in the Fortran 77 programming language.[92]

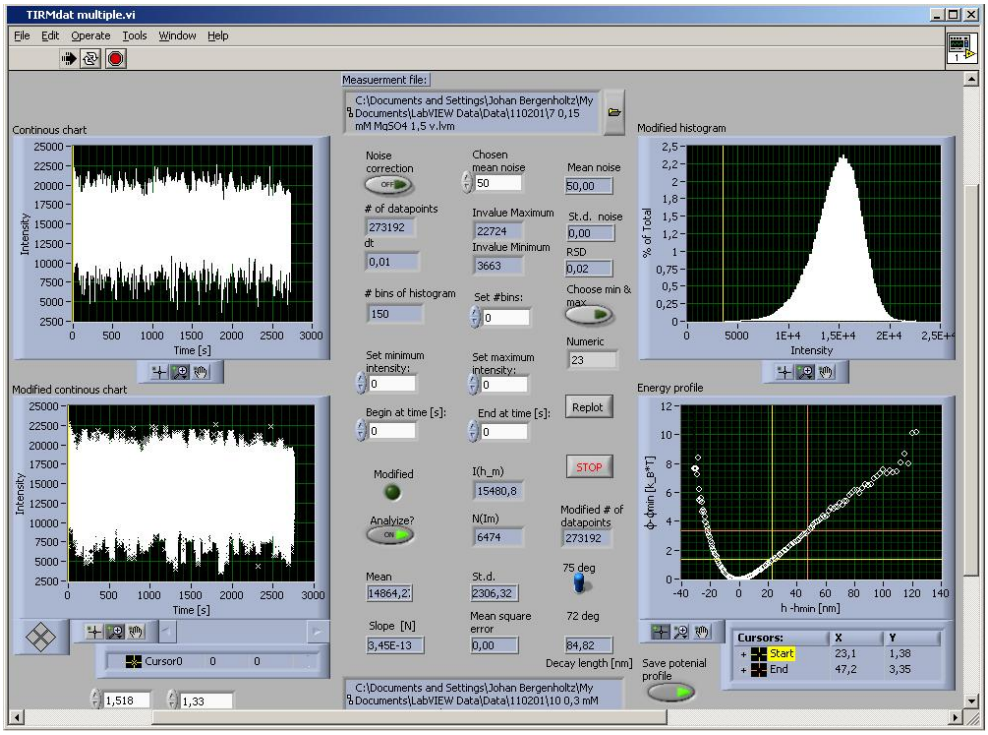

Figure 4.7: Graphic user interface of the data post-treatment program created in LabVIEW. The top-left graph shows the untreated measurement data while the bottom-left shows the raw data after being modified, such as shortened or trimmed of some extreme intensity values. The top-right graph shows the histogram of the intensities for a specified number of bins that can be changed in the program and the bottom-right graph shows the calculated interaction energy profile in accordance with equation 4.4.

4.3.1 A simple interaction potential

For the purpose of illustration, we consider a system, extensively studied by TIRM,[30,93] consisting of a charge-stabilized spherical colloidal particle dispersed in a monovalent electrolyte solution. When the separation distance is large, which is especially in the case at low salt concentrations, the vdW attraction can be more or less neglected which makes the fitting process much easier. In this case the total interaction energy ϕ_{tot} measured in TIRM can be divided in to two parts, the electrostatic free energy ϕ_{el} and the gravitational energy ϕ_G, according to

$$\phi_{tot}(h) = \phi_{el}(h) + \phi_G(h). \tag{4.5}$$

The expression for the gravitational energy is the following simple expression:

$$\phi_G = \frac{4\pi}{3}a^3(\rho_c - \rho_s)gh = Gh, \tag{4.6}$$

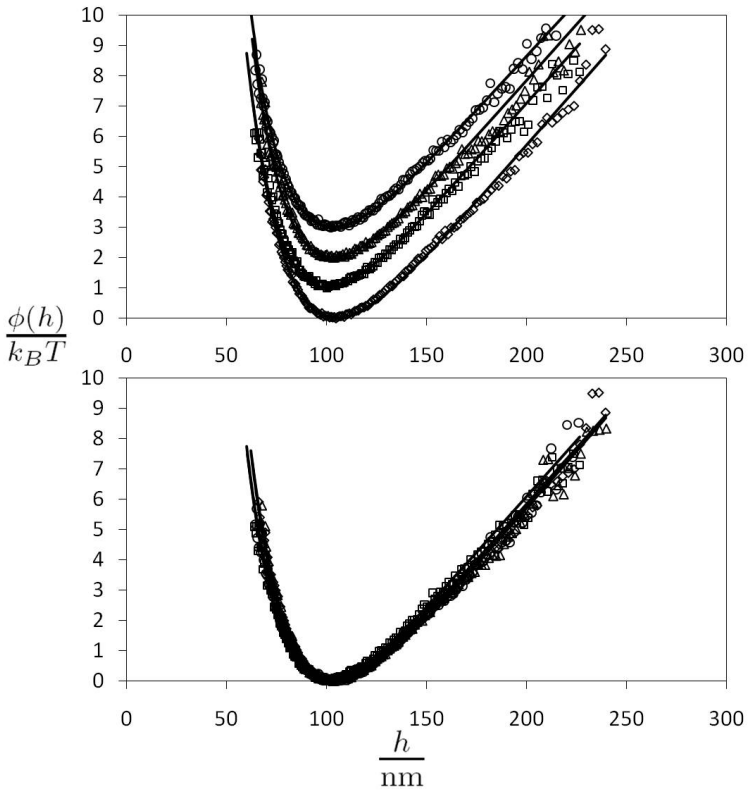

Figure 4.8: Both graphs show results of four consecutive TIRM measurements of a polystyrene particle with expected diameter of 10 μm in 0.2 mM NaCl solution, which calculated with equation (2.3) gives a Debye length of 21 nm. The top graph shows the four measurements differentiated with one k_BT apart. The solid lines are non-linear least-squares fits of the measurement data using equation (4.9) giving fit results with screening lengths ranging between 19.5 to 21 nm and a diameter between 10.1 and 10.2 μm.

where a is the radius of the particle, ρ_c is the density of it, ρ_s is the density of the solvent, and g is the gravitational constant. As described in section 2.2.1, linear superposition and Derjaguin's approximation describe the electrostatic interaction very well in such a system[35,30,94] and the resulting electrostatic potential is then given by equation (2.14), which can be simplified to

$$\phi_{el} = B \exp(-\kappa h). \tag{4.7}$$

Using the expressions in equations (4.6) and (4.7) in equation (4.5) and identifying the minimum interaction energy $\phi(h_m)$ needed in equation (4.4), we find that

$$B = \frac{G}{\kappa} \exp(\kappa h_m). \tag{4.8}$$

Using equations (4.5)-(4.8) in the left-hand-side of equation (4.4), we obtain

$$\frac{\phi(h) - \phi(h_m)}{k_B T} = \frac{G}{\kappa k_B T}\{\exp[-\kappa(h - h_m)] - 1\} + \frac{G}{k_B T}(h - h_m) \qquad (4.9)$$

One of the first proofs of TIRMs reliability has been to measure this interaction potential with great accuracy.[30,95,87] Figure 4.8 shows a measurement of a polystyrene particle from a batch with manufacturer-specified average diameter of 10 ± 0.2 μm in a 0.2 mM NaCl solution and a fit of the measurement using equation (4.9), which agrees very well with the expected values.

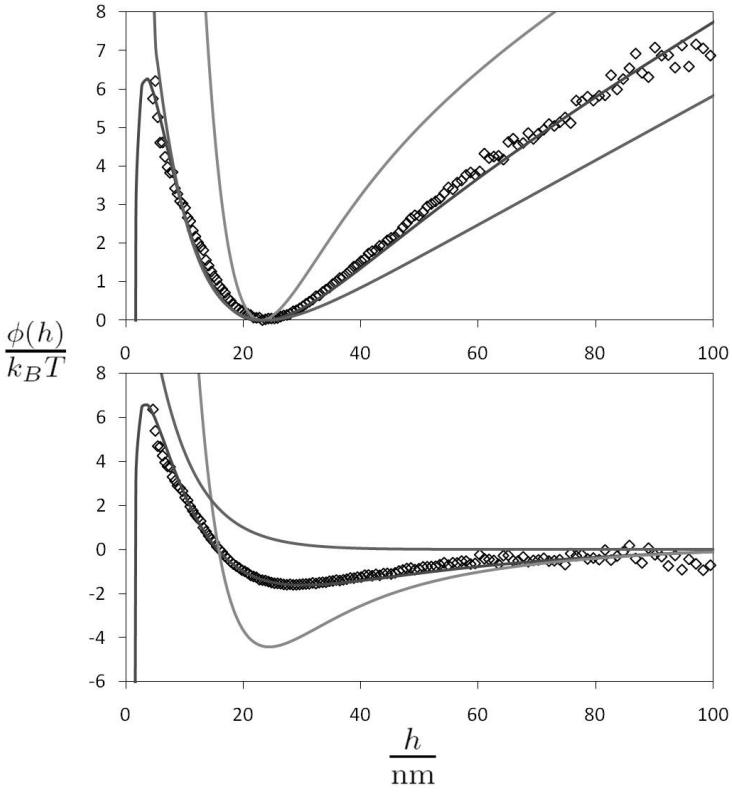

Figure 4.9: Both graphs show fits of a TIRM measurement at higher salt concentration, with the difference between the fits being due to either excluding the vdW interaction, including it but disregarding surface roughness or modeling surface roughness by using the approach of Walz et al.[49] The lower panel shows the same result but, with the weight of the particle subtracted.

4.3.2 Including van der Waals interactions

For particles that are closer to the surface, the vdW interaction cannot be omitted without deteriorating the quality of the fit. However, as discussed in section 2.3 including the vdW interaction is difficult, especially as it has been

seen in TIRM measurements that without considering surface roughness of the glass surface and the colloidal particle, the magnitude of the vdW interaction will clearly be overestimated.[53,51,49,96]This can be seen in figure 4.9 where ex-

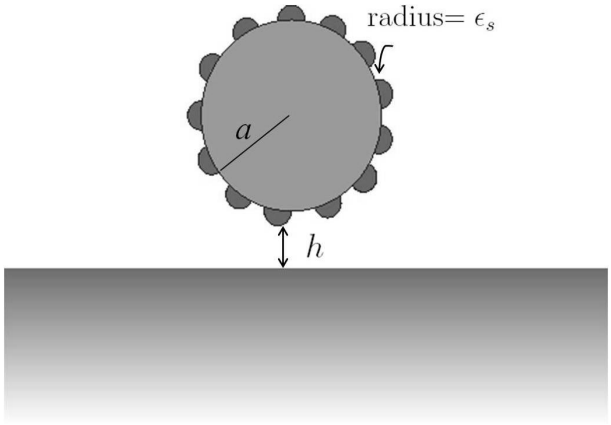

Figure 4.10: Schematic of the roughness model in accordance with work of Walz et al.[52,53,49] where surface roughness is modeled as hemispherical asperities of radius ϵ_s.

cluding the vdW interaction results in a poor fit but including it for smooth surfaces significantly overestimates the strength of the attraction. Different ways of incorporating surface roughness, which weakens the vdW interaction, have been suggested by Prieve et al.[51,96] and Walz et al.[52,53,49] In the fit seen in figure 4.9 and in Paper II, the vdW interaction was included as a combination of an expression given by Czarnecki et al.[97] for the interaction between a smooth sphere and a smooth semi-infinite wall and an expression for the interaction of hemispherical asperities as obtained by Walz et al.,[52,53,49] which reads in full as

$$\begin{aligned}\phi_{\mathrm{vdW}}(h) \;=\; & H_{123}\Big\{\frac{2.45\lambda}{60\pi}\Big(\frac{h-a}{h^2}-\frac{h+3a}{(h+2a)^2}\Big)-\frac{2.17\lambda^2}{720\pi^2}\Big(\frac{h-2a}{h^3}-\frac{h+4a}{(h+2a)^3}\Big)\\ & +\frac{0.59\lambda^3}{5040\pi^3}\Big(\frac{h-3a}{h^4}-\frac{h+5a}{(h+2a)^4}\Big)\\ & +n\Big(\frac{2.45\lambda a}{30}\Big)\Big[\frac{\epsilon_s^2}{2h^2}+\ln\Big(\frac{h}{h-\epsilon_s}\Big)-\frac{\epsilon_s}{h-\epsilon_s}\Big]\\ & -n\Big(\frac{2.17\lambda^2 a}{360\pi}\Big)\Big[\frac{\epsilon_s^2}{h^3}-\frac{1}{h}+\frac{1}{h-\epsilon_s}-\frac{\epsilon_s}{(h-\epsilon_s)^2}\Big]\\ & -n\Big(\frac{0.59\lambda^3 a}{840\pi^2}\Big)\Big[\frac{\epsilon_s^2}{2h^4}-\frac{1}{6h^2}+\frac{1}{6(h-\epsilon_s)^2}-\frac{\epsilon_s}{3(h-\epsilon_s)^3}\Big]\Big\},\end{aligned} \tag{4.10}$$

where, as seen in figure 4.10, a is the radius of the colloidal sphere, ϵ_s is the asperity radius and n is the number density of asperities. As discussed for equations (2.21) and (2.22), λ is known as the intrinsic electronic oscillation

wavelength of the atoms and in our work it was determined through "calibration" against Lifshitz theory. The above equation, but for smooth flat surfaces, was matched to the equivalent Lifshitz result including screening of the zero-frequency term. The fitted values for λ against κ^{-1} is given in table 4.1. We found a relation between λ and κ^{-1} given by the following equation:

$$\lambda = 86.2 + 43.6 \tanh\left[3.8(\log_{10}\kappa^{-1} - 1.04)\right]. \tag{4.11}$$

The values in table 4.1 plotted with the curve obtained by this equation can be seen in figure 4.11.

Table 4.1: This table gives fitted λ values against the Debye screening length κ^{-1}. λ is the intrinsic electronic oscillation wavelength of the atoms and is used to get the right decay properties of the vdW interaction given in (4.10) when retardation as well as screening is included, compared with the Lifshitz theory given in equation (2.18).

κ^{-1}/nm	λ/nm	κ^{-1}/nm	λ/nm
100	131	12	93
50	129.5	10	76
30	126	8	66
20	120	5	50
15	108	1	41

In Paper II we chose to set the asperity radius to 30 nm and the surface coverage to 10 %, numbers that were within the set of values used by Walz et al.[52,53,49] It can be seen in figure 4.9 that reasonably good fits are obtained using these parameters.
In Paper III TIRM measurements were made with particles with 4 layers of decreasing refractive index, going from the core to the outer-most layer. The vdW interaction between these particles and the plane glass wall was modeled as core-single shell particles with two non-retarded Hamaker constants. Furthermore, we chose to use equation (2.17) to describe the interaction between the spherical cores with the surface. For the shell with the lower refractive index we chose the expression given by Tadmor[98] for a thin spherical shell interacting with a semi-infinite wall, which is

$$\phi_{\text{sh-p,vdW}}(h) = -\frac{H_{123}}{6}\Big(\frac{a}{h} - \frac{a}{h+t} - \ln\Big[\frac{h}{h+t}\Big]\Big), \tag{4.12}$$

where t is the thickness of the shell of the particle and a is the radius of the whole particle. Replacing the four-shell structure by a single shell is an approximation and a compromise between having a realistic model and keeping the number of fitting parameters to a minimum. It should be noted, however,

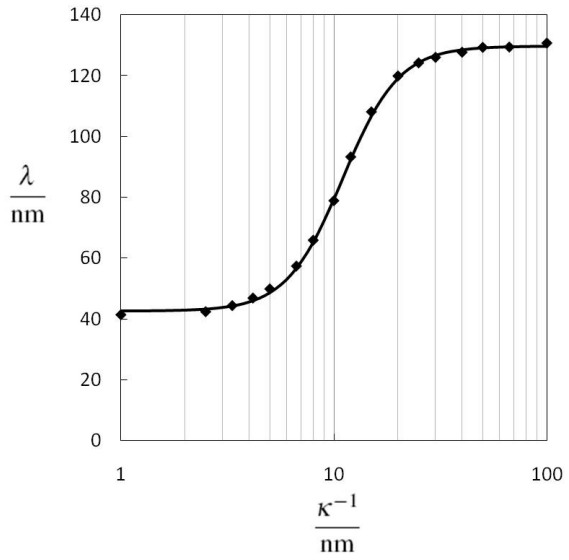

Figure 4.11: The graph shows the fit obtained by using equation (4.11) on table 4.1. λ is known as the intrinsic electronic oscillation wavelength of the atoms. By varying its value, equation (4.10) is made to decay as the more rigorous and numerically calculated Lifshitz equation given in (2.18), and thus allows for including the effects of screening and retardation in the analytical expression.

that the composition of the shells is such as to result in a rather abrupt transition between the refractive indices of the polystyrene core and the fluorinated outer-most layer.

CHAPTER 5

SYNTHESIS OF PARTICLES

In this chapter a review is given of the synthesis work that was done for Paper III and paper IV. In both cases the objective was to synthesize low refractive index particles.

5.1 Synthesis of fluorinated microparticles

Three different sorts of fluorinated particles were synthesized. Two of the implemented synthesis routes were meant to give micrometer sized particles, to be used as single spherical particles to be measured on in the TIRM setup. The third group was meant to be fairly monodisperse particles of high concentration, which were to be used as depletant particles in TIRM measurements for our work with Paper IV. The fluorinated monomers used were 2,2,3,3,4,4,4-

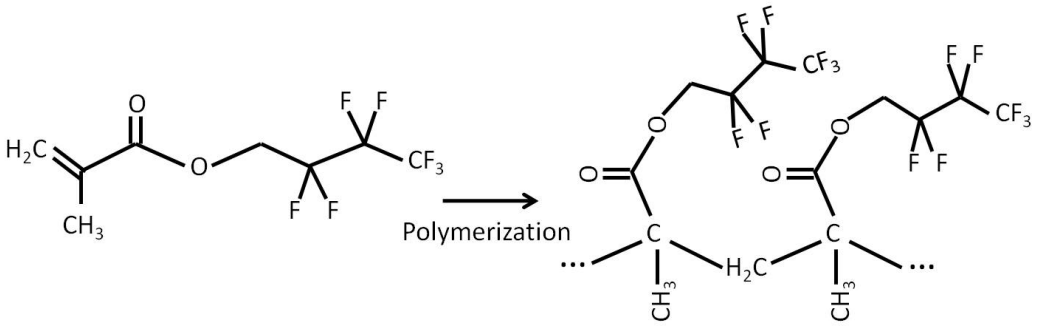

Figure 5.1: Skeletal diagram of 2,2,3,3,4,4,4- heptafluorobutyl methacrylate and its polymerization scheme.

heptafluorobutyl methacrylate (HFBMA, ≈97 %, Alfa Aesar), which contained

Figure 5.2: The synthesis setup is shown here.

20-50 ppm hydroquinone for stabilization during storage. To remove the stabilizing hydroquinone, columns of inhibitor remover for hydroquinone were used (Sigma Aldrich). The same inhibitor remover columns could be used in removing the 4-tertbutylcatechol inhibitor which stabilized the styrene monomers ($\geq$ 99 %, Sigma Aldrich) that were used in synthesizing the multilayered particles. Different initiator chemicals were used during different synthesis procedures, but the polymerization scheme for the HFBMA monomers to poly-(HFBMA) (PHFBMA) presumably proceeds as shown in figure 5.1.
The basic setup of the synthesis process can be seen in figure 5.2. The reactions were carried out in two- or three-necked flasks, submerged in an oil bath. The temperature of the reaction solution was controlled and monitored by a combined hotplate/magnetic stirrer with temperature and stir-rate feedback. One neck of the flask was connected to a reflux condenser which was cooled by a closed circuit circulating water bath.

5.1.1 Synthesis of the micrometer size homogenous fluorinated latex spheres

For the synthesis of the homogenous fluorinated latex spheres we tried first to follow the recipe of Koenderinck et al.[99] However this resulted in particles less than 1 μm sized spheres which is too small to be used to measure on in TIRM. We therefore tried instead to carry out the synthesis as much as possible in accordance with work of Konno et al.,[100,101] who have done work on making surfactant-free, micrometer size monodisperse polystyrene spheres. We hopped that using HFBMA monomers instead of styrene would still yield similar results.
Unfortunately four hours into the synthesis process we noticed that the added

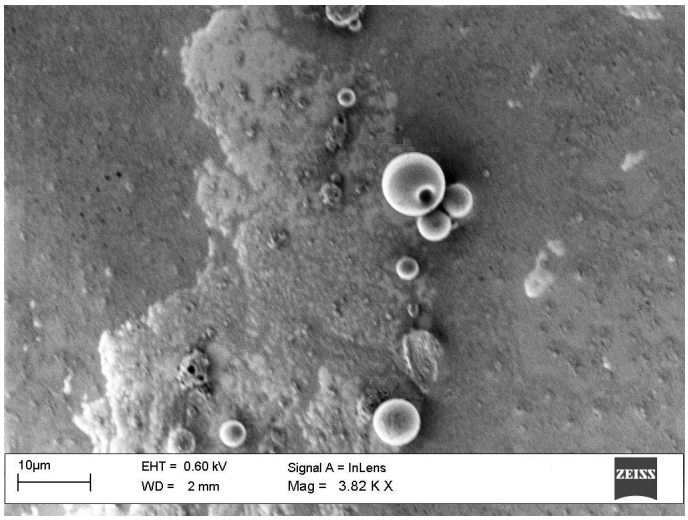

Figure 5.3: Pictures taken in SEM of the PHFBMA particles that were synthesized. The largest particle in the picture has a diameter of 9 μm.

monomers, which made about 20 % of the reaction solution, had phase separated and subsequently gelled at the bottom of the reaction vessel. We therefore aborted the continuation of the polymerization and recovered the particle solution that had formed. Dynamic light scattering (DLS) measurement showed that most of the particles formed during this short time were around 30 nm in diameter. However viewing the particles in scanning electron microscopy (SEM) showed that much larger particles were also formed with some as large as around 10 μm in diameter, as can be seen in 5.3. Polydispersity is not a problem for TIRM as TIRM measurements are done on single particles. Once a suitable particle is found other particles can be pumped out of the cell while the chosen particle is kept in place by the optical tweezer. However the low refractive index of the particles, which is around 1.38, makes the particles scatter insufficiently to be usable in our TIRM setup.

5.1.2 Synthesis of multilayered spheres

To obtain particles that scatter more and yet posses the properties of a low refractive index particle, multilayered particles were synthesized instead, with an outer-most layer consisting of fluorinated polymer. First, polystyrene (PS) particles were prepared which were subsequently used as seeds in the following layering steps. In each step the ratio of HFBMA monomers compared to styrene monomers was increased until the outer-most layer consisted of 100 % PHFBMA. The procedure of Alteheld et al.[102] was followed in preparing the multilayered particles, except in the synthesis of the PS core where their procedure was modified somewhat in accordance with work of Konno et al.[100,101]

Table 5.1: Table over the synthesis recipe used at each layering step, where the starting solution volume contained around 1 weight % seed particles from the previous synthesis step.

Layer	start volume (mL)	styrene (g)	HFBMA (g)	KPS (mL)	AIBN (mg)	EGDMA (μL)	mβc (mg)
1	60	6.36	0.99	20	147	13	200
2	40	0.78	4.43	0	104	6.4	100
3	40	0	5.636	0	112.7	6.4	100

In synthesis of the PS core, only KPS initiator ($K_2S_2O_8$, $\geq$ 99.99 %, Sigma Aldrich) was used but the approach of Konno et al.[100,101] was adopted by having a buffer concentration of 10 mM NH_4Cl and NH_4OH and to replace 3/4 of the reaction volume with fresh buffer and styrene monomers 8 h after the initiation of the polymerization process. In preparing the PS particles, 80 mL buffer solution mixed with 40 mL styrene monomers containing 0.2 mL cross-linking agent ethylene glycol dimethacrylate (EGDMA, $\geq$ 98 %) was prepared and bubbled with nitrogen gas while stirring at 1000 rpm for about 30 minutes. After that the temperature was raised to 65°C, while having the mixture under nitrogen gas flow. When the desired temperature was achieved, 15 mL of a the initiator solution containing 4.25 mM KPS was added to the reaction flask while decreasing the stirring speed to 300 rpm. The reaction was allowed to proceed during 8 h, after which three fourths of the reactant solution was removed from the reaction flask and the flask was subsequently charged with an equivalent amount of styrene monomers, buffer solution and initiator solution to compensate for the removed reactants.
In using the PS particles as seeds in the next steps of our synthesis of applying layers, the procedure of Alteheld et al.[102] was followed as much as possible, using the prescribed chemicals at similar concentrations. Initiators KPS and 2,2'-azobis(2-methylpropionitrile) (AIBN, $\geq$ 98%, Acros organics) as well as chemicals methyl-β-cyclodextrin (mβc, average M_n = 1310, 1.6- 2.0 CH_3 groups per unit anhydroglucose, Sigma Aldrich) and EGDMA were used in the layering process in accordance with the work of Alteheld et al.[102]
In the layering process we tried to decrease the refractive index of the outer shells in 3 steps, where the last shell would be made up of only fluorinated polymers, while the intermediate steps were made of mixtures of styrene and HFBMA with increasing amount of HFBMA. Too large of a difference in composition of subsequent layers were shown to result in non-spherical particles, where several polystyrene particles would become encapsulated into one. This is believed to be due to the high difference in interfacial tension between the layers.[102] The three layers were mixed as to contain in weight:weight ratio 87:13, 15:85, 0:100 styrene and HFBMA monomers respectively. Alteheld et

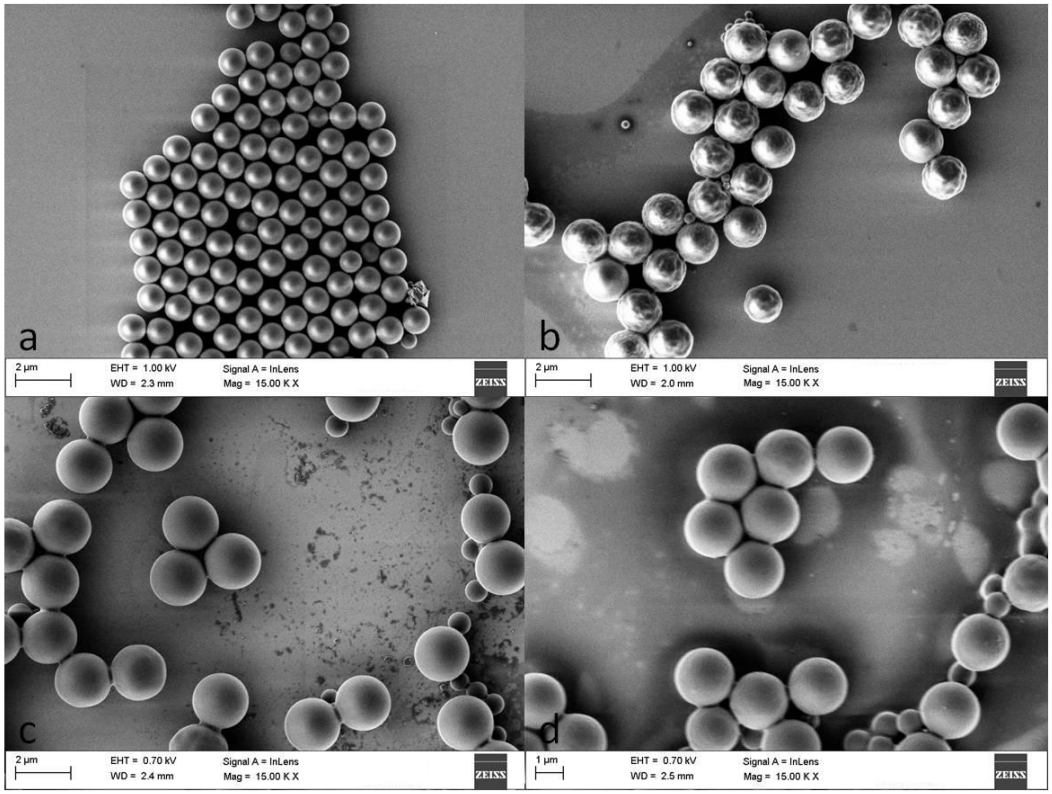

Figure 5.4: Pictures taken in SEM of the multilayered particles with a showing the core polystyrene particles. For (b), (c) and (d), mixtures of styrene:HFBMA monomers with weight ratio of 83:17, 15:85 and 0:100 were used respectively. See 5.5 for the evolution of the mean diameter of the larger particles.

al.[102] showed in their work using proton magnetic resonance microscopy that this procedure gives layers containing almost the same ratio of content between PS and PHFBMA. We assume this to be true in our case also without further investigation.

Table 5.1 gives the proportions of the material that was used at each layering step. The layering proceeded with seed particles from the previous stage, containing around 1 weight % particles, as well as mβc being charged into the reaction flask and heated to 80°C, while stirred at a speed of around 300 rpm. The methyl-β-cyclodextrin was used to increase the solubility of HFBMA monomers. The monomer mixture, cross-linking agent EGDMA and the initiator AIBN were mixed together and were introduced to the reaction flask at a speed of about 0.1 mL/min. Parallel to this, in the first layering step, 20 mL of a 0.2 mM KPS initiator solution was introduced to the reaction flask during the same amount of time that the monomers were introduced into the reaction flask, i.e. at a speed rate of about 0.26 mL/min. The reaction was then allowed to proceed for 3 h after the feeding stage was completed.

Figure 5.4 shows the achieved result from the polystyrene seeds seen in (a) to

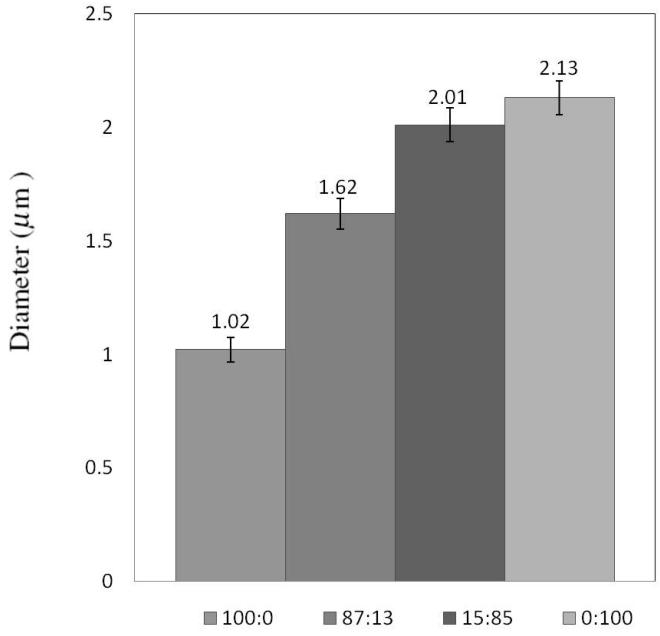

Figure 5.5: The measured average size of the bigger particles seen in 5.4. The ratio below each diagram shows the styrene:HFBMA monomers ratio added during the synthesis.

the end result seen in (d.) The average size of the primary particles can be seen in figure 5.5, where the size of more than 50 larger primary particles were averaged. The secondary nucleation seen first in figure 5.4 (c) can probably be avoided with adjustments in the synthesis procedure.

5.1.3 Synthesis of depletant particles

The depletants with low refractive index were prepared following the recipe of Koenderink et al.[99] First, 40 mL of mili-Q water (18 MΩ cm) was bubbled with nitrogen gas while heated to 70 °C during one hour. After that 8 mL of the monomer was introduced in the reaction flask and emulsified at stirring speed of 1000 rpm during 30 minutes. A glass-coated magnet was used for the stirring. The stirring speed was lowered to 300 rpm as 2 mL of the initiator solution was introduced into the reaction flask. The initiator solution contained 8.5 mM KPS and an equivalent amount of 7.6 mM $NaHSO_3$. The polymerization was allowed to proceed during 14 h. Some coagulum was formed that was removed by filtration.
About 40 mL of depletant dispersion was retained with a particle concentration of approximately 10 weight %. The weight concentration was determined in this case by measuring the weight of about 0.2 mL of the sample in a glove box with argon atmosphere so that the salt in the solution would not absorb water

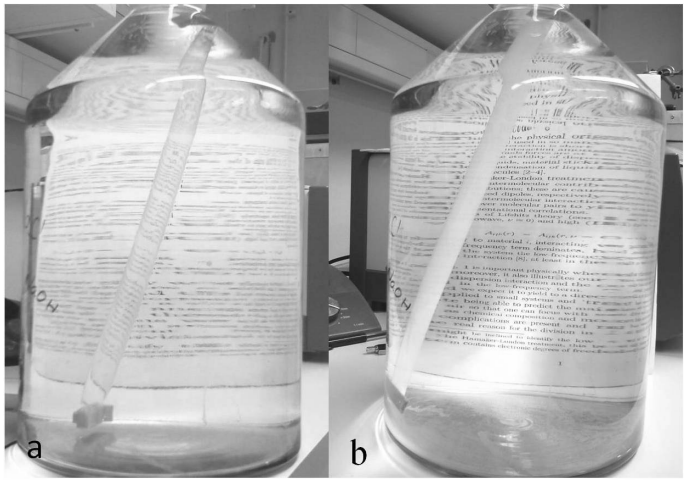

Figure 5.6: The pictures show the dialysis of the depletants against 0.074 mM NaOH water solution after they have been used in a TIRM measurement. In picture (a) the solvent in the dialysis tube is the 30:70 volume % DMSO:H_2O mixture used in our measurement, which will have a refractive index of around 1.38, matching the refractive index of the depletant particles. Hence the content of the dialysis tube is clear. Within few hours however most of DMSO has diffused out of the dialysis tube and the sample is turbid as can be seen in (b).

from the surrounding air. SEM measurements in combination with DLS measurements were done as to decide the size and polydispersity of the fluorinated latex spheres.
The reason we synthesized depletant particles with low refractive index was the ability to match the refractive index of the particles with the surrounding solution and hence avoid scattering from the depletant particles. Figure 5.6 shows the dialysis of the depletant solution after a measurement series where in (a) the solvent in the dialysis tube is 30:70 volume % DMSO:H_2O mixture which will have a refractive index of around 1.38, matching the refractive index of the depletant particles. In (b) however few hours have passed and dialysis has replaced most of the solution around the depletant particles in the dialysis tube with water which has a refractive index of around 1.33. The mismatch in the refractive index, however not that big, makes the solution in the dialysis tube to appear milky turbid due to scattering from the high concentration particle solution.

CHAPTER 6

SUMMARY OF PAPERS

Paper I

In this paper we used the in-house-built TIRM instrument to investigate colloidal interactions in two different non-ionic surfactant solutions, octylphenoxy polyethoxy ethanol (commonly known as Triton X-100) and penta(ethylene glycol) dodecylether (commonly known as $C_{12}E_5$). We have measured the interaction energy between a spherical polystyrene colloid and a glass surface for different concentrations of the non-ionic surfactants while still being within the micellar L_1 phase. We focus on concentrated micellar solutions.
Triton X-100 and $C_{12}E_5$ are two of the most used and studied non-ionic surfactants. One of the important areas of use for non-ionic surfactants is in colloidal systems, where non-ionic surfactants are used to provide steric stabilization.[103] Steric stabilization is achieved by the adsorption of the non-ionic surfactants to the surface of the particles which will thus prevent the colloids from coming close enough for the van der Waals attraction to become too strong. There are however other effects that are less studied and understood. For instance, there have been reports of long-range forces in concentrated $C_{12}E_5$ solutions.[15] Figure 6.1 shows one of the measurements where we observed a drastic change in the interaction energy between a charge-stabilized polystyrene particles with a diameter of about 10 μm and the glass surface. It was observed that at sufficiently high surfactant concentration the particles became attached physically to the surface. It was concluded that this force was caused by formation of some bridging structure between the colloid and the surface. The effect seen in figure 6.1 was seen in our measurements for $C_{12}E_5$ concentration above 6 mM. The same particles suspended in Triton X-100 solutions do not show this phenomena. However, a factor of some interest revealed in our measurements is that the as-supplied Triton X-100, as well as the as-supplied $C_{12}E_5$, contains some salt or other ionic species. Use of an ion-exchange resin removes these

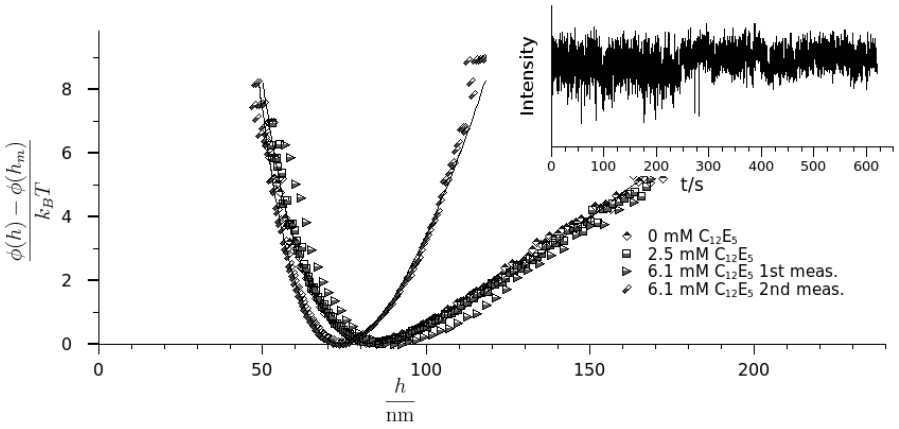

Figure 6.1: TIRM measurement on a spherical polystyrene particle with a diameter of about 10 μm in aqueous $C_{12}E_5$ solutions with a background electrolyte concentration of 0.6 mM NaCl. There is no significant change between the 0 and 2.5 mM $C_{12}E_5$ measurements. The raw intensity data for the first measurement at 6.1 mM $C_{12}E_5$ is shown in the inset. The triangle symbols show the interaction energy that is obtained when the first part ($0 < t < 210$ s) of that measurement is analyzed. The second measurement at 6.1 mM $C_{12}E_5$ represents the second part of the inset after the particle seemingly is attached to the surface. The fit used for the attached data uses the expression from equation (4.9) with additional terms for a parabolic potential which include fit parameters for an equilibrium distance and a spring constant.

salts, after which it was found that Triton X-100 neither affects the long-range electrostatic interaction, as had been reported in the past,[87] nor led to particle attachment.

Paper II

The effect of salts with different properties, including multivalent salts, was investigated with the TIRM instrument. Incorporating vdW interaction when analyzing the measurement interaction potentials become increasingly important as the salt concentration is increased. Using the expected Hamaker constat for the interaction between the glass plate and our probe particle, which for the most part was polystyrene particles with a diameter of 10 μm, overestimate the vdW interaction (see figure 4.9), as has been observed in past measurements.[49,96] This discrepancy has been suggested to be caused by surface roughness, and we incorporate the effect of surface roughness, following Walz et al.[49] via equation (4.10).
Figure 6.2 shows the result for all the different salts that were measured on,

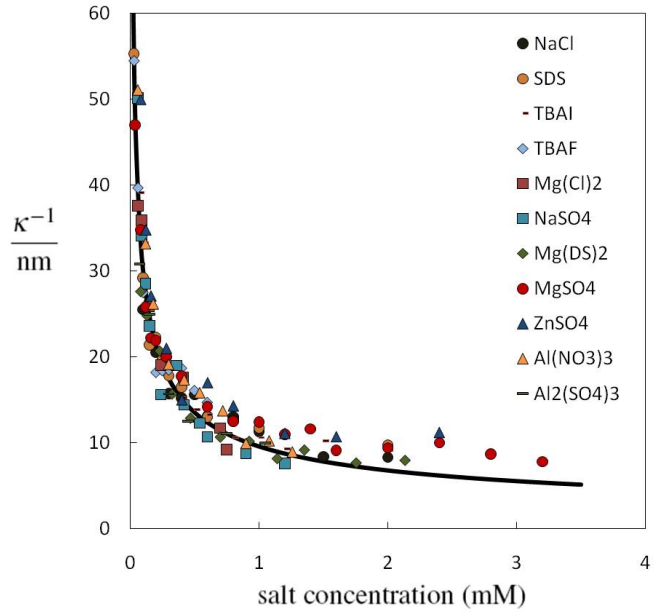

Figure 6.2: The fitted Debye length of the salts that were measured in paper III. The concentration of the different salts was recalculated to the equivalent 1:1 salt concentration.

recalculated as the equivalent amount of a 1:1 salt. The results for most salts follow, within the margin of error, the expected Debye length quite well. However the screening length of the 2:2 salts at higher salt concentration are greater than the Debye length. This is qualitatively consistent with theory based on the primitive model of electrolytes,[104] but the magnitude of the deviation is greater than predicted for these rather low salt concentrations.

Paper III

For this paper latex particles with a strongly scattering polystyrene core and an outer shell of a refractive index near that of water were synthesized. The effect of the refractive index of the solvent on the vdW interaction was studied in water/DMSO and water/DMF mixtures. Figure 6.3 shows SEM pictures taken of the particles. TIRM measurements in aqueous NaCl solutions showed that higher salt concentrations than previously reported for TIRM with polystyrene particles could be reached, indicating weaker vdW interactions. Qualitatively similar results were obtained for a solvent refractive index close to matching that of the particle shell. However, for a solvent refractive index between those of the glass surface and the shell of the particle only repulsive interactions were observed before the particle got attached to the surface. Addition of salt initially screened the interaction, but a second addition had no effect on

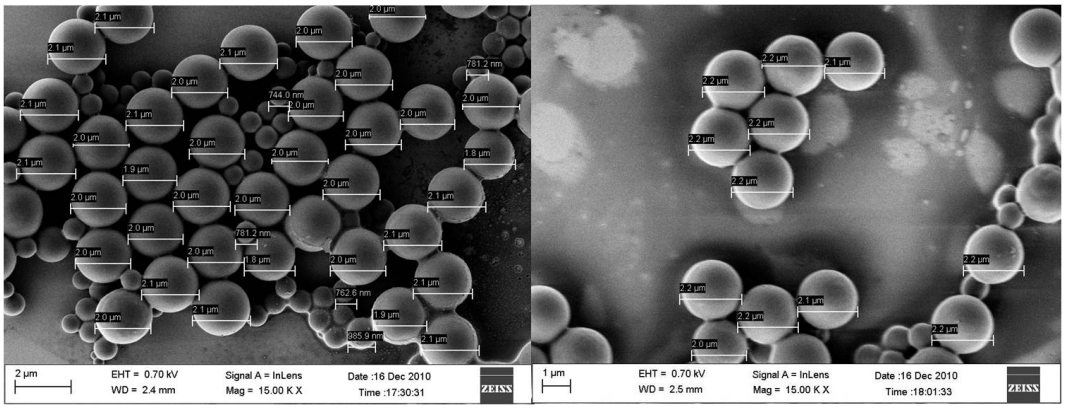

Figure 6.3: SEM pictures of the synthesized particles used for measurements in paper III. The picture on the left shows SEM picture of the particles at the stage where the multilayered particles had two layers on the polystyrene core, with the outer-most layer having a weight fraction of 15:85 styrene:HFBMA monomers and the right picture shows the particles having a third layer, made of 100 % PHFBMA.

the interaction. This result can be explained qualitatively by a net repulsive vdW interaction even though the solvent mixture is polar. In all cases the particles become attached to the surface, which is due to a lower electric surface potential in these solvent mixtures and the vdW interaction being given by its non-screened form for very small separations.

Paper IV

Low-refractive-index particles were used as depletant particles in TIRM measurements in refractive-index-matched DMSO/water mixtures. This allowed for TIRM measurements with a minimum of scattering contamination from the depletant particles. TIRM measurements were carried out to study depletion-like interactions caused by these particles. In this case the depletant particles, the large colloidal microsphere, and glass surface were all charged and effects of depletant and salt concentration were systematically investigated.
To fit the measurement data, a model based on a 3-component OZ equation with a hybrid HNC-MSA closure was solved. In this case the interactions between particles were assumed to be given by screened Coulomb potentials, see equation 2.28. Figure 6.4 shows the result for the highest measured depletant concentration and lowest salt concentration. The data could only be described by the model quantitatively if a smaller depletant diameter and a higher salt concentration were used in the model. As shown in figure 6.4, using values closer to experimental conditions can be achieved to some extent by modifying the cross-interaction by including a so-called non-additivity parameter

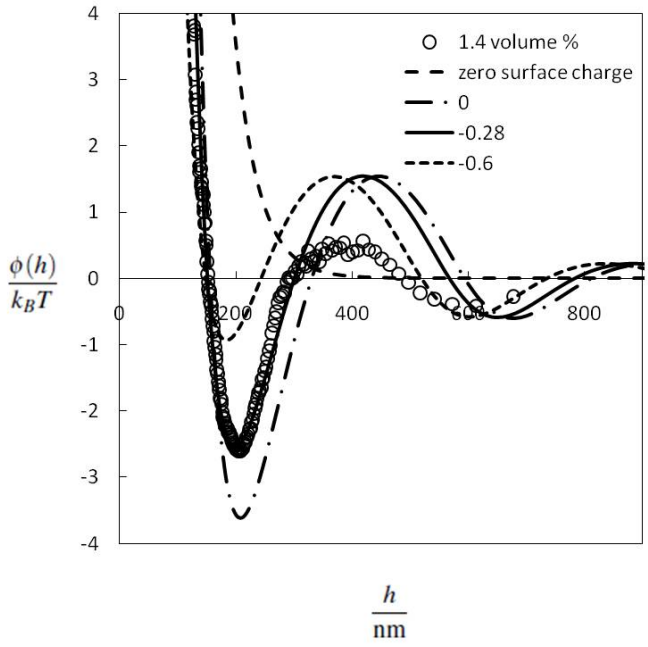

Figure 6.4: The normalized interaction potential is shown as a function of separation distance for 1.4 volume % of depletant spheres. The first solid line curve shows a calculated interaction potential when the depletant particles are modeled as hard spheres, according to the parameters that are given as system D in table 1 of Paper IV. The other solid line curves show calculations with different Δ values, where the other parameters are given as the system E entry in table 1 of Paper IV.

Δ. Increasingly negative values of Δ shifts the repulsive barrier to smaller separations in qualitative agreement with the TIRM data.

Paper V

In this paper small angle scattering data from oil-in-water microemulsions with a non-ionic surfactant shell was analyzed. We modeled the colloidal interactions between the microemulsions with an effective hard-sphere interaction which could differ from the particle diameter. By solving the Ornstein Zernike equation (see equation (2.24)) using the Percus Yevick closure (see equation (3.10)), analytical solutions for the scattering intensity, given in equation (3.14), for polydisperse core-shell and multilayered hard spheres were obtained. The polydispersity in the system was modeled by a continuous Schulz distribution (equation (3.15)).
The analytical expressions obtained makes for rapid evaluations of $I(q)$ for interacting spheres with some internal structure. By setting the shell thicknesses

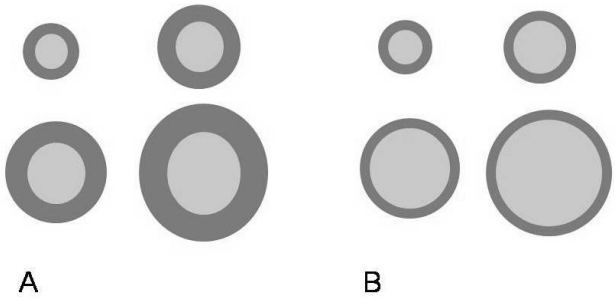

Figure 6.5: Model A is depicted in (A), where the shell thickness changes in proportion to the particle diameter. (B) represents model B, where the shell thickness is constant while the core diameter is governed by Schulz distribution.

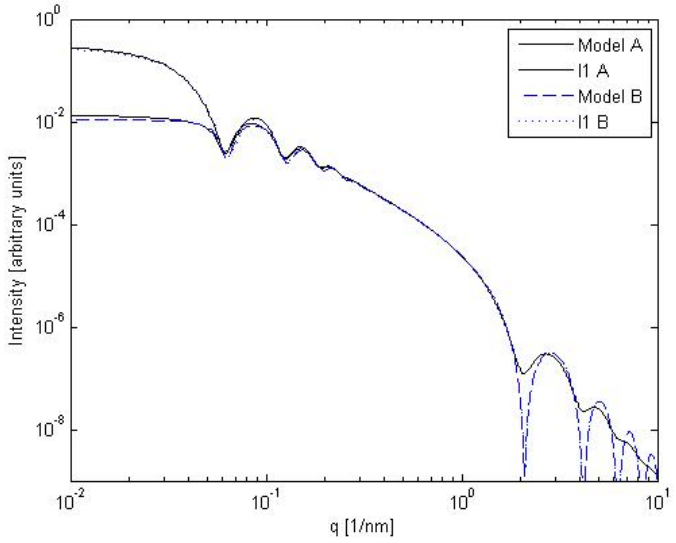

Figure 6.6: Calculation with both models A and B for a vesicle-like particle distribution. The mean total particle radius is set to 50 nm and the mean shell thickness or the constant shell thickness in model B is set to 4 nm. It can be seen that for model B, the constant shell thickness gives more distinct minimas at certain q values. Also the result of I_1 for respective model is plotted.

of the particles to zero and the effective diameter of the hard-sphere potential equal to the actual particle diameter, the expression of Griffith et al.[84] for homogenous hard-sphere particles is again obtained.
To have an effective hard-sphere potential that differs from the actual particle diameter is in line with common practice in accounting for extra repulsions.[105] Two types of internal particle structuring is considered, consistent with what has been proposed in past.[106,107] Solutions for the form factor, which is given in I_1, have been derived previously for these two types of core-shell particles by Hayter[106] and Bartlett and Ottewill.[107] Hayter derived solutions for I_1

given that the shell thickness is proportional to the particle diameter, which we call model A, while Bartlett and Ottewill derived solutions for the form factor where the shell thickness is constant, which we call model B. We have obtained solutions for both cases as well as the equivalent for multilayered particles. The difference between the models is illustrated in figure 6.5. Figure 6.6 shows scattering intensities calculated for both models for core-shell, vesicle-like particles, i.e. particles where the contrast of the core is the same as the surrounding solvent. It can be seen in figure 6.6 that the difference between the two models becomes apparent with more distinct minimas due to constant shell thicknesses which will give destructive interferences at q values that are multiples of $2\pi/\delta$, where δ is the shell thickness.
Using our analytical model the best fits for the water, n-decane, $C_{12}E_5$ microemulsion droplets were obtained for an effective hard-sphere potential with a diameter of 1.065 times bigger than the actual particle diameter. This indicates a somewhat more long reaching interaction than the actual particle diameter which can be attributed to extra hydration of the microemulsion droplets.

CHAPTER 7

CONCLUSIONS AND FUTURE OUTLOOK

A range of different types of colloidal interactions have been covered in this thesis. It is important for the continued progress of colloid science and the vast area for its applicability to check theoretical results by comparing with experiments. With this in mind the main part of this thesis has been devoted to the use of TIRM for this purpose. TIRM is a very sensitive method which gives a direct measure of the interactions between a colloidal sphere and a flat surface.

In Paper I, effects of two different types of non-ionic surfactants, $C_{12}E_5$ and Triton X-100, on the sphere-wall interaction were investigated for concentrations well above the critical micelle concentration (CMC) but still well below any lamellar liquid crystalline phase. After removal of residual ionic species it was shown that Triton X-100 solutions had little effect on long-range interactions at concentrations up to 285 times the CMC, whereas polystyrene and silica particles were found to get elastically tethered at concentrations around 85 times CMC. It is notable that $C_{12}E_5$, in contrast to Triton X-100, forms worm-like micelles with increasing concentration within the micellar phase, and the physical attachment was tentatively attributed to a bridging surfactant structure. This work could be extended by similar studies of other non-ionic surfactant solutions that form worm-like micelles and attempting to identify what kind of structure causes the tethering.

In Paper II TIRM was used to study the effects of different salts, including different ionic surfactants, on the EDL interaction, which necessitated modeling the vdW interaction. In the somewhat limited ionic strength interval that is measurable with TIRM, we found a significant deviation from DH theory for the 2:2 salts $MgSO_4$ and $ZnSO_4$. Whereas other multivalent electrolytes and surfactants behaved as point charges for which screening lengths were reasonably well described by the Debye length, the screening lengths for the 2:2 salts were considerably longer than the Debye length. While this result agrees qualita-

tively with theoretical predictions based on the primitive model of electrolytes, the magnitude of the deviation was found to be larger than predicted. For future work it would be interesting to be able to measure screening lengths at higher salt concentrations where deviations from DH theory is expected. This would require a few improvements of the technique, such as a better signal-to-noise ratio. Furthermore, using the particles synthesized for the work done in Paper III, which exhibit a much weaker vdW interaction, would allow for measurements at higher salt concentrations.

Multi-layered particles with an outer layer of low refractive index were synthesized in Paper III in order to explore vdW interactions. When the refractive index of the DMSO/water solvent was brought to a value intermediate between the glass wall and the outer-most layer of the particle, large discrepancies between measured screening lengths and Deybe lengths were observed such that addition of salt was found to have no effect on the interaction. This response can be explained by a net repulsive vdW interaction even though the solvent is polar. However more experiments should be done to verify the mechanism and to pinpoint under what conditions it occurs.

Fluorinated, low-refractive-index particles were used at higher concentrations as depletant particles in measuring the interaction between a larger polystyrene microsphere and a glass surface for larger depletant-microsphere size ratios than before. The effect of salt and depletant particle concentration was determined systematically. For larger concentrations of depletant and/or low salt concentrations a deep attractive minimum followed by a longer range repulsive barrier were observed. A model based on integral equation theory was shown to capture these effects qualitatively. The integral equation theory used is largely untested and should in future work be compared against computer simulations. In addition, the modeling showed that better agreement between data and theory may be obtained by altering the cross-interactions in the system, which could be explored further.

Integral equation theory was also used to model small-angle X-ray scattering data from microemulsion droplets covered by shells made up by the nonionic surfactant $C_{12}E_5$. It was shown that the droplets could be well described as polydisperse core-shell spheres with an effective hard-sphere interaction. Even though the experiments are well described by the analytical expressions derived, it would be interesting to verify the actual shape and interactions of these particles with other experimental methods because others have reached different conclusions in the past.

ACKNOWLEDGEMENTS

Johan Bergenholtz: supervisor, with open door policy, that always have shown patience, kindness and humbleness in sharing his vast knowledge in all areas of physical chemistry, but also with regards to English grammar and spelling.

Jonas Nordström: colleague, but first and foremost friend who most recently has acted as a crisis hotline number regarding problems with LaTeX.

Alpo Karpinen: for saving my work PC from crashing several times over and for helping me setting up the computers that connect to the TIRM instrument.

Benny Lönn: for all the work he has done in customizing instrument parts for the in-house built TIRM.

Sture Nordholm: for reassuring me during the first years that it is quite normal with a slower startup period and the existence of the "ketchup effekten".

Jenny Perez Holmberg: for co-sharing the responsibility for the Zetasizer and all the shared hours in the cave.

Patrick Steegstra: for teaching me about SEM and about why Holland should have had won against Spain.

Jonas Fredriksson: for playing the bad cop during the gas lab interrogations.

Anna Reymer: my roommate who I also consider as my taller little sister.

Mother and brother: for being great at being my mother and brother.

Past and present colleagues at FK: no names mentioned, no one forgotten, thank you to those who have helped me in my work and all the others, thank you for all the laughs and the good times we have shared during coffee breaks and all these graduation and spring parties.

BIBLIOGRAPHY

[1] D. F. Evans and H. Wennerström, *The colloidal domain.* Wiley-VCH, 2nd ed., 1999.

[2] T. J. Schmidt, M. Noeske, H. A. Gasteiger, R. J. Behm, P. Britz, and H. Bonnemann, "PtRu alloy colloids as precursors for fuel cell catalysts," *J. Electrochem. Soc.*, vol. 145, no. 3, p. 925, 1998.

[3] A. S. Arico, P. Bruce, J.-M. T. B. Scrosati, and W. van Schalkwijk, "Nanostructured materials for advanced energy conversion and storage devices," *Nature Materials*, vol. 4, p. 366, 2005.

[4] K. Kataoka, A. Harada, and Y. Nagasaki, "Block copolymer micelles for drug delivery: design, characterization and biological significance," *Adv. Drug Del. Rev.*, vol. 47, no. 1, p. 113, 2001.

[5] P. N. Pusey and W. van Megen, "Phase behavior of concentrated suspensions of nearly hard colloidal spheres," *Nature*, vol. 320, p. 340, 1986.

[6] K. N. Pham, A. M. Puertas, J. Bergenholtz, S. U. Egelhaaf, A. Moussaid, P. N. Pusey, A. B. Schofield, M. E. Cates, M. Fuchs, and W. C. K. Poon, "Multiple glassy states in a simple model system," *Science*, vol. 296, no. 5565, p. 104, 2002.

[7] D. Frenkel, "Colloidal Systems: Playing Tricks with Designer "Atoms"," *Science*, vol. 296, no. 5565, p. 65, 2002.

[8] J. N. Israelachvili and D. Tabor, "The measurement of van der Waals dispersion forces in the range 1.5 to 130 nm," *Proc. Royal Soc. London A*, vol. 331, no. 1584, p. 19, 1972.

[9] J. N. Israelachvili and G. E. Adams, "Measurement of forces between two mica surfaces in aqueous electrolyte solutions in the range 0-100 nm," *J. Chem. Soc. Faraday Trans. 1*, vol. 74, p. 975, 1978.

[10] J. N. Israelachvili, "Forces between surfaces in liquids," *Adv. Colloid Interf. Sci.*, vol. 16, no. 1, p. 31, 1982.

[11] J. N. Israelachvili and P. M. McGuiggan, "Forces between surfaces in liquids," *Science*, vol. 241, no. 4867, p. 795, 1988.

[12] P. M. Claesson, J. C. Eriksson, C. Herder, B. A. Bergensthl, E. Pezron, I. Pezron, and P. Steinus, "Forces between non-ionic surfactant layers," *Faraday Dis. Chem. Soc.*, vol. 90, p. 129, 1990.

[13] P. Richetti and P. Kekicheff, "Direct measurement of depletion and structural forces in a micellar system," *Phys. Rev. Lett.*, vol. 68, p. 1951, Mar 1992.

[14] W. A. Ducker, T. J. Senden, and R. M. Pashley, "Measurement of forces in liquids using a force microscope," *Langmuir*, vol. 8, no. 7, p. 1831, 1992.

[15] M. W. Rutland and T. J. Senden, "Adsorption of the poly(oxyethylene) nonionic surfactant $C_{12}E_5$ to silica: a study using atomic force microscopy," *Langmuir*, vol. 9, no. 2, p. 412, 1993.

[16] Y. H. Tsao, D. F. Evans, and H. Wennerstrom, "Long-range attractive force between hydrophobic surfaces observed by atomic force microscopy," *Science*, vol. 262, no. 5133, p. 547, 1993.

[17] T. J. Senden, C. J. Drummond, and P. Kekicheff, "Atomic force microscopy: Imaging with electrical double layer interactions," *Langmuir*, vol. 10, no. 2, p. 358, 1994.

[18] J. Dong and G. Mao, "Direct study of $C_{12}E_5$ aggregation on mica by atomic force microscopy imaging and force measurements," *Langmuir*, vol. 16, no. 16, p. 6641, 2000.

[19] J. Y. Walz, "Measuring particle interactions with total internal reflection microscopy," *Curr. Opin. Colloid Interf. Sci.*, vol. 2, no. 6, p. 600, 1997.

[20] D. C. Prieve, " Measurement of colloidal forces with TIRM ," *Adv. Colloid Interf. Sci.*, vol. 82, p. 93, 1999.

[21] S. G. Bike, "Measuring colloidal forces using evanescent wave scattering," *Curr. Opin. Colloid Interf. Sci.*, vol. 5, no. 1-2, p. 144, 2000.

[22] S. Biggs, D. C. Prieve, and R. R. Dagastine, "Direct comparison of atomic force microscopic and total internal reflection microscopic measurements in the presence of nonadsorbing polyelectrolytes," *Langmuir*, vol. 21, no. 12, p. 5421, 2005.

[23] J. C. Crocker, J. A. Matteo, A. D. Dinsmore, and A. G. Yodh, "Entropic attraction and repulsion in binary colloids probed with a line optical tweezer," *Phys. Rev. Lett.*, vol. 82, p. 4352, May 1999.

[24] P. L. Biancaniello and J. C. Crocker, "Line optical tweezers instrument for measuring nanoscale interactions and kinetics," *Rev. Sci. Instrum.*, vol. 77, p. 113702, 2006.

[25] S. Tanimoto, H. Matsuoka, and H. Yamaoka, "Direct estimation of dynamic characteristics and interaction potential of latex particles interacting with a glass surface by evanescent wave light-scattering microscope method," *Colloid Polym. Sci.*, vol. 273, p. 1201, 1995.

[26] S. Tanimoto, H. Matsuoka, H. Yamauchi, and H. Yamaoka, "Direct estimation of the electrostatic interaction between colloidal particle and chemically modified glass surface by the evanescent wave light scattering microscope method," *Colloid Polym. Sci.*, vol. 277, p. 130, 1999.

[27] J. K. Dreyer, K. Berg-Srensen, and L. Oddershede, "Improved axial position detection in optical tweezers measurements," *Appl. Opt.*, vol. 43, p. 1991, 2004.

[28] P. M. Hansen, J. K. Dreyer, J. Ferkinghoff-Borg, and L. Oddershede, "Novel optical and statistical methods reveal colloid-wall interactions inconsistent with dlvo and lifshitz theories," *J. Colloid Interf. Sci.*, vol. 287, no. 2, p. 561, 2005.

[29] D. C. Prieve and B. M. Alexander, "Hydrodynamic measurement of double-layer repulsion between colloidal particle and flat plate," *Science*, vol. 231, no. 4743, p. 1269, 1986.

[30] F. L. D. C. Prieve and F. Lanni, "Brownian motion of a hydrosol particle in a colloidal force field," *Faraday Dis. Chem. Soc.*, vol. 83, p. 297, 1987.

[31] W. Brown, R. Rymden, J. Van Stam, M. Almgren, and G. Svensk, "Static and dynamic properties of nonionic amphiphile micelles: Triton X-100 in aqueous solution," *J. Phys. Chem.*, vol. 93, no. 6, p. 2512, 1989.

[32]

[33] P. Debye and E. Hückel, "The theory of electrolytes. I. Lowering of freezing point and related phenomena," *Physikalische Zeitschrift*, vol. 24, p. 185, 1923.

[34] R. Kjellander, "The basis of statistical thermodynamics." Lecture notes, University of Gothenburg, 1991.

[35] E. J. W. Verwey and J. T. G. Overbeek, *Theory of the stability of lyophobic colloids*. Amsterdam: Elsevier, 1948.

[36] H. H. von Grünberg and E. C. Mbamala, "Charged colloids near interfaces," *J. Phys.: Condens. Matter*, vol. 13, no. 21, p. 4801, 2001.

[37] J. Israelachvili, *Intermolecular and surface forces*. Academic Press, 3 ed., 2011.

[38] G. Bell, S. Levine, and L. McCartney, "Approximate methods of determining the double-layer free energy of interaction between two charged colloidal spheres," *J. Colloid Interf. Sci.*, vol. 33, no. 3, p. 335, 1970.

[39] H. B. G. Casimir and D. Polder, "Influence of Retardation on the London-van der Waals Forces," *Nature*, vol. 158, p. 787, 1946.

[40] H. Hamaker, "The london-van der waals attraction between spherical particles," *Physica*, vol. 4, no. 10, p. 1058, 1937.

[41] E. Lifshitz, "The theory of molecular attractive forces between solids," *Soviet Phys. JETP*, vol. 2, p. 73, 1956.

[42] I. E. Dzyaloshinskii, E. M. Lifshitz, and L. P. Pitaevskii, "General theory of van der Waals' forces," *Soviet Physics Uspekhi*, vol. 4, no. 2, p. 153, 1961.

[43] D. C. Prieve and W. B. Russel, "Simplified predictions of Hamaker constants from Lifshitz theory," *J. Colloid Interf. Sci.*, vol. 125, no. 1, p. 1, 1988.

[44] B. W. Ninham, V. A. Parsegian, and G. H. Weiss, "On the macroscopic theory of temperature-dependent van der waals forces," *J. of Stat. Phys.*, vol. 2, p. 323, 1970.

[45] V. A. Parsegian and G. H. Weiss, "Spectroscopic parameters for computation of van der Waals forces," *J. Colloid Interf. Sci.*, vol. 81, no. 1, p. 285, 1981.

[46] C. M. Roth and A. M. Lenhoff, "Improved parametric representation of water dielectric data for lifshitz theory calculations," *J. Colloid Interf. Sci.*, vol. 179, no. 2, p. 637, 1996.

[47] L. Bergstr "Hamaker constants of inorganic materials," *Adv. Colloid Interf. Sci.*, vol. 70, p. 125, 1997.

[48] J. H. Schenkel and J. A. Kitchener, "A test of the Derjaguin-Verwey-Overbeek theory with a colloidal suspension," *Trans. Faraday Soc.*, vol. 56, p. 161, 1960.

[49] J. Y. Walz, L. Suresh, and M. Piech, "The effect of nanoscale roughness on long range interaction forces ," *J. Nanopart. Res.*, vol. 1, p. 99, 1999.

[50] J. Czarnecki and T. Dabros, "Attenuation of the van der Waals attraction energy in the particle/semi-infinite medium system due to the roughness of the particle surface," *J. Colloid Interf. Sci.*, vol. 78, no. 1, p. 25, 1980.

[51] M. A. Bevan and D. C. Prieve, "Direct measurement of retarded van der Waals attraction," *Langmuir*, vol. 15, no. 23, p. 7925, 1999.

[52] L. Suresh and J. Y. Walz, "Effect of surface roughness on the interaction energy between a colloidal sphere and a flat plate," *J. Colloid Interf. Sci.*, vol. 183, no. 1, p. 199, 1996.

[53] L. Suresh and J. Y. Walz, "Direct measurement of the effect of surface roughness on the colloidal forces between a particle and flat plate," *J. Colloid Interf. Sci.*, vol. 196, no. 2, p. 177, 1997.

[54] J. Israelachvili, *Intermolecular and surface forces*. Academic Press, 2 ed., 1991.

[55] A. Parsegian, *Van der Waals forces*. Cambridge univesity press, 2006.

[56] A. Milling, P. Mulvaney, and I. Larson, "Direct measurement of repulsive van der waals interactions using an atomic force microscope," *J. Colloid Interf. Sci.*, vol. 180, no. 2, p. 460, 1996.

[57] A. Meurk, P. F. Luckham, and L. Bergström, "Direct measurement of repulsive and attractive van der waals forces between inorganic materials," *Langmuir*, vol. 13, no. 14, p. 3896, 1997.

[58] S. woo Lee and W. M. Sigmund, "Repulsive van der Waals forces for silica and alumina," *J. Colloid Interf. Sci.*, vol. 243, no. 2, p. 365, 2001.

[59] A. A. Feiler, L. Bergstrom, and M. W. Rutland, "Superlubricity using repulsive van der waals forces," *Langmuir*, vol. 24, no. 6, p. 2274, 2008.

[60] J. N. Munday, F. Capasso, and V. A. Parsegian, "Measured long-range repulsive Casimir-Lifshitz forces," *Nature*, vol. 457, p. 170, 2009.

[61] J. Traube, "Konzentrierung von Kautschukmilchsften," *Gummi Zeitung*, p. 434, 1925.

[62] S. Asakura and F. Oosawa, "On interaction between two bodies immersed in a solution of macromolecules," *J. Chem. Phys.*, vol. 22, p. 1255, 1954.

[63] A. Vrij, "Polymers at interfaces and the interactions in colloidal dispersions," *Pure Appl. Chem.*, vol. 48, p. 471, 1976.

[64] R. J. Klein, S. Zhang, S. Dou, B. H. Jones, R. H. Colby, and J. Runt, "Modeling electrode polarization in dielectric spectroscopy: Ion mobility and mobile ion concentration of single-ion polymer electrolytes," *J. Chem. Phys.*, vol. 124, no. 14, p. 144903, 2006.

[65] D. Kleshchanok, R. Tuinier, and P. R. Lang, "Direct measurements of polymer-induced forces," *J. Phys.: Condens. Matter*, vol. 20, no. 7, p. 073101, 2008.

[66] J. M. Mendez-Alcaraz and R. Klein, "Depletion forces in colloidal mixtures," *Phys. Rev. E*, vol. 61, p. 4095, 2000.

[67] J. P. Hansen and I. R. McDonald, *Theory of simple liquids*. San Diego: Academic Press, 3rd ed., 2006.

[68] D. C. Prieve and J. Y. Walz, "Scattering of an evanescent surface wave by a microscopic dielectric sphere," *Appl. Opt.*, vol. 32, no. 9, p. 1629, 1993.

[69] H. Chew, D. S. Wang, and M. Kerker, "Elastic scattering of evanescent electromagnetic waves," *Appl. Opt.*

[70] E. Eremina, N. Grishina, Y. Eremin, L. Helden, and T. Wriedt, "Total internal reflection microscopy with a multilayered interface: a light scattering model based on a discrete sources method," *J. Opt. A: Pure Appl. Opt.*, vol. 8, no. 11, p. 999, 2006.

[71] L. Helden, E. Eremina, N. Riefler, C. Hertlein, C. Bechinger, Y. Eremin, and T. Wriedt, "Single-particle evanescent light scattering simulations for total internal reflection microscopy," *Appl. Opt.*, vol. 45, no. 28, p. 7299, 2006.

[72] C. Hertlein, N. Riefler, E. Eremina, T. Wriedt, Y. Eremin, L. Helden, and C. Bechinger, "Experimental verification of an exact evanescent light scattering model for TIRM," *Langmuir*, vol. 24, no. 1, p. 1, 2008.

[73] A. Guinier and G. Fournet, *Small angle scattering of X-rays*. Wiley, New York, 2nd ed., 1955.

[74] O. Spalla, "General theorems in small-angle scattering," in *Neutrons, X-rays and light scaterring Methods Applied to soft condensed matter* (P. Lindner and T. Zemb, eds.), North-Holland, Elsevier Science, 2002.

[75] R. Klein, "Interacting colloidal suspensions," in *Neutrons, X-rays and light scaterring Methods Applied to soft condensed matter* (P. Lindner and T. Zemb, eds.), North-Holland, Elsevier Science, 2002.

[76] M. S. Wertheim, "Exact solution of the Percus-Yevick integral equation for hard spheres," *Phys. Rev. Lett.*, vol. 10, no. 8, p. 321, 1963.

[77] E. Thiele, "Equation of state for hard spheres," *J. Chem. Phys.*, vol. 39, no. 2, p. 474, 1963.

[78] J. L. Lebowitz, "Exact solution of generalized Percus-Yevick equation for a mixture of hard spheres," *Phys. Rev. Lett.*, vol. 133, no. 4A, p. A895, 1964.

[79] R. J. Baxter, "Ornstein–Zernike relation and Percus–Yevick approximation for fluid mixtures," *J. Chem. Phys.*, vol. 52, no. 9, p. 4559, 1970.

[80] L. Blum and G. Stell, "Polydisperse systems. I. Scattering function for polydisperse fluids of hard or permeable spheres," *J. Chem. Phys.*, vol. 71, no. 1, p. 42, 1979.

[81] L. Blum and G. Stell, "Erratum: Polydisperse systems. I. Scattering function for polydisperse fluids of hard or permeable spheres," *J. Chem. Phys.*, vol. 72, no. 3, p. 2212, 1980.

[82] A. Vrij, "Mixtures of hard spheres in the Percus–Yevick approximation. Light scattering at finite angles," *J. Chem. Phys.*, vol. 71, no. 8, p. 3267, 1979.

[83] S. R. Aragón and R. Pecora, "Theory of dynamic light scattering from polydisperse systems," *J. Chem. Phys.*, vol. 64, no. 6, p. 2395, 1976.

[84] W. L. Griffith, R. Triolo, and A. L. Compere, "Analytical scattering function of a polydisperse Percus-Yevick fluid with Schulz- (Γ) distributed diameters," *Phys. Rev. A*, vol. 35, no. 5, p. 2200, 1987.

[85] B. M. Alexander and D. C. Prieve, "A hydrodynamic technique for measurement of colloidal forces," *Langmuir*, vol. 3, no. 5, p. 788, 1987.

[86] M. A. Bevan and D. C. Prieve, "Forces and hydrodynamic interactions between polystyrene surfaces with adsorbed PEO-PPO-PEO," *Langmuir*, vol. 16, p. 9274, 2000.

[87] M. A. Brown and E. J. Staples, "Measurement of absolute particle-surface separation using total internal reflection microscopy and radiation pressure forces," *Langmuir*, vol. 6, no. 7, p. 1260, 1990.

[88] D. Kleshchanok, *Polymer-induced colloidal interaction:measured by direct and indirect methods*. PhD thesis, RWTH Aachen University, 2007.

[89] A. Ashkin, "Acceleration and trapping of particles by radiation pressure," *Phys. Rev. Lett.*, vol. 24, no. 4, p. 156, 1970.

[90] A. Ashkin, J. M. Dziedzic, J. E. Bjorkholm, and S. Chu, "Observation of a single-beam gradient force optical trap for dielectric particles," *Opt. Lett.*, vol. 11, no. 5, p. 288, 1986.

[91] J. Y. Walz and D. C. Prieve, "Prediction and measurement of the optical trapping forces on a microscopic dielectric sphere," *Langmuir*, vol. 8, no. 12, p. 3073, 1992.

[92] W. H. Press, S. A. Teukolsky, W. T. Vetterling, and B. P. Flannery, *Numerical Recipes in FORTRAN*. Cambridge, 2nd ed., 1992.

[93] H. H. von Grünberg, L. Helden, P. Leiderer, and C. Bechinger, "Measurement of surface charge densities on Brownian particles using total internal reflection microscopy," *J. Chem. Phys.*, vol. 114, no. 22, p. 10094, 2001.

[94] H. H. von Grünberg and E. C. Mbamala, "Colloidal suspensions at dielectric interfaces," *J. Phys.: Condens. Matter*, vol. 12, no. 50, p. 10349, 2000.

[95] S. Bike and D. Prieve, "Measurements of double-layer repulsion for slightly overlapping counterion clouds," *Int. J. Multiphase Flow*, vol. 16, no. 4, p. 727, 1990.

[96] R. Dagastine, "Calculation of van der Waals forces with diffuse coatings: Applications to roughness and adsorbed polymers," *J. Adhesion*, vol. 80, p. 365, 2004.

[97] J. Czarnecki, "Van der Waals attraction energy between sphere and half-space," *J. Colloid Interf. Sci.*, vol. 72, no. 2, p. 361, 1979.

[98] R. Tadmor, "The London-van der Waals interaction energy between objects of various geometries," *J. Phys.: Condens. Matter*, vol. 13, p. L195, 2001.

[99] G. H. Koenderink, S. Sacanna, C. Pathmamanoharan, M. Rasa, and A. P. Philipse, "Preparation and properties of optically transparent aqueous dispersions of monodisperse fluorinated colloids," *Langmuir*, vol. 17, no. 20, p. 6086, 2001.

[100] S. Gu, S. Inukai, and M. Konno, "Preparation of monodisperse, micron-sized polystyrene particles with an amphoteric initiator in soapfree polymerization," *J. Chem. Eng. of Japan*, vol. 35, no. 10, p. 977, 2002.

[101] Y. Yamada, T. Sakamoto, S. Gu, and M. Konno, "Soap-free synthesis for producing highly monodisperse, micrometer-sized polystyrene particles up to 6 μm," *J. Colloid Interf. Sci.*, vol. 281, no. 1, p. 249, 2005.

[102] A. Alteheld, I. Gourevich, L. M. Field, C. Paquet, and E. Kumacheva, "Multilayer polymer particles with periodic modulation in refractive index," *Macromolecules*, vol. 38, no. 8, p. 3301, 2005.

[103] M. Romero-Cano, A. Martin-Rodrguez, and F. de las Nieves, "Colloidal stabilization and destabilization of a carboxyl latex by adsorption of Triton X-100," *Macromolecular Symposia*, vol. 151, p. 427, 2000.

[104] R. Kjellander and D. J. Mitchell, "Dressed-ion theory for electrolyte solutions: A debye–hückel-like reformulation of the exact theory for the primitive model," *J. Chem. Phys.*, vol. 101, no. 1, p. 603, 1994.

[105] U. Olsson and P. Schurtenberger, "Structure, interactions, and diffusion in a ternary nonionic microemulsion near emulsification failure," *Langmuir*, vol. 9, no. 12, p. 3389, 1993.

[106] J. B. Hayter, "Determination of the structure and dynamics of micellar solutions by neutron small-angle scattering," in *Physics of amphiphiles: micelles, vesicles and microemulsions* (V. Degiorgio and M. Corti, eds.), p. 59, Proc. Intl. School of Physics, Enrico Fermi, North-Holland, Amsterdam, 1985.

[107] P. Bartlett and R. H. Ottewill, "A neutron scattering study of the structure of a bimodal colloidal crystal," *J. Chem. Phys.*, vol. 96, no. 4, p. 3306, 1992.